

Unusual electronic ordering in the pseudogap phase of underdoped cuprate superconductors

Xiang Li^{1,2}, Minghuan Zeng^{3,*}, Yu Lan⁴, Huaiming Guo⁵, and Shiping Feng^{2,1†}

¹*School of Physics and Astronomy, Beijing Normal University, Beijing 100875, China*

²*Department of Physics, Faculty of Arts and Sciences, Beijing Normal University, Zhuhai 519087, China*

³*College of Physics, Chongqing University, Chongqing 401331, China*

⁴*College of Physics and Electronic Engineering, Hengyang Normal University, Hengyang 421002, China and*

⁵*School of Physics, Beihang University, Beijing 100191, China*

The pseudogap phase of the underdoped cuprate superconductors harbours diverse manifestations of different ordered electronic-states, and then these ordered electronic-states coexist or compete with superconductivity. Here starting from the microscopic electron propagator, the nature of the ordered electronic-states in the pseudogap phase is investigated within the T -matrix approach. This T -matrix is derived in terms of the inverse of matrix for various kinds of a single impurity, and then is used to evaluate the local density of states (LDOS) by the involvement of all the quasiparticle excitations and scattering processes. It is shown that a number of the anomalous properties in the underdoped cuprate superconductors is directly correlated to the opening of the normal-state pseudogap: (i) the structure of the microscopic octet scattering model generated by the normal-state pseudogap is essentially the same both in the superconducting (SC)-state and pseudogap phase, which naturally leads to that the quasiparticle scattering interference octet phenomenology observed in the SC-state exists in the pseudogap phase; (ii) however, the spectral weight at around the antinodal region in the SC-state is gapped out completely by both the SC gap and normal-state pseudogap, while it in the pseudogap phase is suppressed partially by the normal-state pseudogap, this directly leads to that the non-dispersive checkerboard charge ordering with a finite wave vector \mathbf{Q} appears in the pseudogap phase only. The theory therefore also shows that the electronic-states affected by the normal-state pseudogap exhibit the LDOS modulation spectrum organization.

PACS numbers: 74.62.Dh, 74.62.Yb, 74.25.Jb, 71.72.-h

I. INTRODUCTION

In spite of over the past three decades of intense research, the cuprate superconductors still hold many mysteries¹⁻³. They are complex systems that exhibit a variety of phases determined not only by temperature, but also by the charge-carrier doping⁴⁻¹¹. This follows from a basic fact that the parent compounds of cuprate superconductors are a Mott insulator¹², which originates from the strong electron correlation¹³, and then superconductivity with the exceptionally high superconducting (SC) transition temperature T_c is obtained by doping charge carriers^{14,15}, where the doping regimes have been classified into the underdoped, optimally doped, and overdoped, respectively⁴⁻¹¹. However, this charge-carrier doping process nearly always introduces some measure of disorder¹⁶⁻¹⁸, leading to that in principle, all cuprate superconductors have naturally impurities, and then the electronic inhomogeneity (then the inhomogeneous quasiparticle distribution) emerges naturally¹⁹⁻²¹. This remarkable evolution from a strongly correlated Mott insulator with the localized electronic-state to a high- T_c superconductor with the delocalized electron pairing-state thus demonstrates unambiguously that the anomalous properties of the electronic inhomogeneity in cuprate superconductors are governed by both the strong electron correlation and impurity scattering^{22,23}.

After intensive studies over three decades, the innumerable experimental observations by using many probes have pointed out that the most of the exotic and unique features of cuprate superconductors are to be found in the normal-state and where the deepest mysteries lie⁴⁻¹¹. In particular, the normal-state in the underdoped regime is characterized by a pseudogap⁴⁻⁹ below the pseudogap crossover temperature T^* large compared to T_c . In addition to the high- T_c SC mechanism, this normal-state pseudogap is the most noteworthy. The normal-state pseudogap depresses partially the electron density of states on the electron Fermi surface (EFS), and then the anomalous properties associated with the opening of the normal-state pseudogap are explained in a natural way. This is also why in the underdoped regime, the phase above T_c but below T^* is labelled as *the pseudogap phase*⁴⁻⁹. Although the electronic inhomogeneity of cuprate superconductors in the pseudogap phase is intrinsic in the nature, the quasiparticles scattering from impurities interfere with one another, which leads to that the inhomogeneous quasiparticle distribution is seeded by the impurity scattering¹⁹⁻²⁹. Experimentally, by virtue of systematic studies using scanning tunneling microscopy/spectroscopy (STM/S) measurement techniques, a number of consequences from the electronic inhomogeneity together with the associated fluctuation phenomena in the pseudogap phase have been identified as³⁰⁻³⁶: (i) the stronger quasiparticle scattering is

detected at around the antinodal region than at around the nodal region, which leads to that the constant energy contour for a finite binding-energy is truncated to form the Fermi arcs centered at around the nodal region with the largest spectral weight located at around the tips of the Fermi arcs, which has been also confirmed by the angle-resolved photoemission spectroscopy (ARPES) experiments^{37–42}. The characteristic features associated with this constant energy contour instability are the emergence of the multiple nearly-degenerate electronic orders^{43–48}, the dramatic change in the line-shape of the energy distribution curve^{48–56}, and the kink in the quasiparticle dispersion^{57–62}. More specially, these tips of the Fermi arcs connected by the scattering wave vectors \mathbf{q}_i construct an *octet scattering model*, which can give a consistent description of the regions of the highest joint density of states^{37–42}; (ii) the modulation of the local density of states (LDOS) in the SC-state appears for the most part to be described by the quasiparticle scattering interference (QSI) caused by the quasiparticle scattering from impurities, where the QSI peaks describe the regions of the highest joint density of states, and are located at the well-defined scattering wave vectors \mathbf{q}_i ($i=1,2,\dots,7$) obeying the *octet scattering model*; (iii) all these QSI signatures detectable in the SC-state^{24–29} survive virtually unchanged into the pseudogap phase. Concomitantly, all seven scattering wave vectors $\mathbf{q}_i(\omega)$, which are dispersive in the SC-state, remain dispersive into the pseudogap phase. In this case, the multiple ordered electronic-states, which emerge in the pseudogap phase above T_c , persist into the SC-state below T_c , and then they coexist and compete with the SC-state^{43–48}; (iv) however, in addition to the QSI octet phenomenology, the unusual checkerboard peaks in the LDOS modulation at a finite scattering wave vector \mathbf{Q} emerge in the pseudogap phase only. In particular, this remarkable checkerboard charge ordering is observed to be non-dispersive, and therefore is a static local charge ordering. These experimental observations therefore provide the firm evidence for the LDOS modulation spectrum organization due to the opening of the normal-state pseudogap.

Although the unusual features of the LDOS modulation in the pseudogap phase^{30–36} have been established experimentally, a complete understanding of these anomalous properties is still unclear, where the crucial questions emerge in the field: (i) why the characteristic of the QSI octet phenomenology observed in the SC-state also appears to remain unchanged upon passing above T_c in the pseudogap phase? (ii) whether the normal-state pseudogap generates the checkerboard charge ordering in the pseudogap phase? In our recent work⁶³, the nature of the LDOS modulation of cuprate superconductors in the SC-state for various kinds of impurities has been investigated within the T -matrix approach, and the obtained results show that (i) the overall feature of the LDOS modulation can be described qualitatively by taking into account the quasiparticle

scattering from a single impurity on the kinetic-energy-driven homogeneous SC-state; (ii) the QSI scattering wave vectors \mathbf{q}_i and the related QSI peak dispersions are internally consistent within the octet scattering model. In this paper, we study the distinct feature of the LDOS modulation in the pseudogap phase along with this line. We identify explicitly that (i) the structure of the SC-state QSI patterns in the LDOS modulation does not undergo any significant change as a function of temperature through T_c to the pseudogap phase. Moreover, as in the SC-state⁶³, the QSI peaks in the pseudogap phase are also dispersive with the dispersion of the QSI peaks being particle-hole symmetric; (ii) the additional checkerboard peaks in the LDOS modulation, which are suppressed strongly in the SC-state by the SC gap, emerge in the pseudogap phase only. In particular, this checkerboard charge ordering is found to be energy-independent. Our results therefore show that the occurrence of the unusual checkerboard charge ordering is intrinsically connected with the opening of the normal-state pseudogap.

This paper is organized as follows. The brief review of the interplay between the pseudogap-state and superconductivity is presented in Section II, where in the kinetic-energy-driven superconductivity, the normal-state pseudogap and SC gap respectively originate from the homogeneous electron normal self-energy in the particle-hole channel and anomalous self-energy in the particle-particle channel, and are evaluated by taking into account the vertex correction. In Section III, we start from the homogeneous electron propagator and the related *microscopic octet scattering model* to derive LDOS in the pseudogap phase within the T -matrix approach, where the T -matrix is calculated accurately for various kinds of a single impurity to include all the quasiparticle excitations and scattering processes. The quantitative characteristics of the LDOS modulation in the underdoped cuprate superconductors are presented in Section IV, where we show that the checkerboard charge-order wave vector in the pseudogap phase obtained from the LDOS modulation is qualitatively consistent with the results observed from the ARPES and STM/S experiments. Finally, we give a brief summary in Sec. V. In Appendix A, we present the accurate calculation of the impurity-induced T -matrix in the pseudogap phase in terms of the method of the inversion of matrix.

II. INTERPLAY BETWEEN PSEUDOGAP-STATE AND SUPERCONDUCTIVITY

A. t - J model with constrained electron

The key common feature in the crystal structure of cuprate superconductors is the presence of the copper-oxide (CuO_2) plane^{14,15}, and then it seems evident that the anomalous properties of cuprate superconductors are

mainly governed by these CuO₂ planes. In this case, as originally suggested by Anderson¹³, the essential physics of the doped CuO₂ plane can be properly modeled with the square-lattice t - J model,

$$H = - \sum_{ll'} t_{ll'} C_{l\sigma}^\dagger C_{l'\sigma} + \mu \sum_{l\sigma} C_{l\sigma}^\dagger C_{l\sigma} + J \sum_{\langle ll' \rangle} \mathbf{S}_l \cdot \mathbf{S}_{l'}, \quad (1)$$

where $C_{l\sigma}^\dagger$ ($C_{l\sigma}$) creates (annihilates) an electron with spin index σ on lattice site l , \mathbf{S}_l is a localized spin operator with its components S_l^x , S_l^y , and S_l^z , and μ is the chemical potential. This t - J model (1) contains two parts: the kinetic energy part consists of the nearest-neighbor (NN) electron hopping term $t_{ll'} = t_{\hat{\eta}} = t$ and the next NN electron hopping term $t_{ll'} = t_{\hat{\tau}} = -t'$, while the magnetic energy part is described by a Heisenberg term with the NN spin-spin antiferromagnetic (AF) exchange coupling J . The summation ll' is taken over all sites l , and for each l , over its NN sites $\hat{\eta}$ and next NN sites $\hat{\tau}$, while the summation $\langle ll' \rangle$ is taken over all the NN pairs. For a convenience in the following discussions, the NN spin-spin AF exchange coupling J and the lattice constant a of the square lattice are set as the energy and length units, respectively. Although the values of J , t , and t' in cuprate superconductors are believed to vary somewhat from compound to compound⁶⁻⁸, however, as a qualitative discussion in this paper, the commonly used parameters are chosen as $t/J = 2.5$ and $t'/t = 0.3$. In particular, when necessary to compare with the experimental data, we set $J = 100\text{meV}$.

The t - J model (1) is subjected to the on-site local constraint that the double electron occupancy of a site by two electrons of opposite spins is not allowed⁶⁴⁻⁶⁷. The physics of the charge-spin separation appears in the fermion-spin theory^{68,69} which starts from the t - J model (1) and enforces the on-site local constraint of no double electron occupancy by decoupling the physical electron into a spinful fermion and a localized spin as,

$$C_{l\uparrow} = h_{l\uparrow}^\dagger S_l^-, \quad C_{l\downarrow} = h_{l\downarrow}^\dagger S_l^+, \quad (2)$$

where the $U(1)$ gauge invariant spinful fermion operator $h_{l\sigma}^\dagger = e^{i\Phi_{l\sigma}} h_l^\dagger$ ($h_{l\sigma} = e^{-i\Phi_{l\sigma}} h_l$) creates (annihilates) a charge carrier on site l , and therefore describes the charge degree of freedom of the constrained electron together with some effects of spin configuration rearrangements due to the presence of the doped charge carrier itself, while S_l^+ (S_l^-) is the $U(1)$ gauge invariant localized spin-raising (spin-lowering) operator, which describes the spin degree of freedom of the constrained electron, and then the on-site local constraint of the no double electron occupancy is always satisfied at each site. Moreover, the collective mode from the spin degree of freedom of the constrained electron can be interpreted as the spin excitation responsible for the spin dynamics of the system, while the constrained electron as a result of the charge-spin recombination of a charge carrier and a localized spin is responsible for the anomalous properties of the electronic-state.

B. Homogeneous electron propagator

Based on the t - J model (1) in the fermion-spin representation, the kinetic-energy-driven superconductivity has been developed⁶⁹⁻⁷³, where the coupling between charge carriers directly from the kinetic energy in the fermion-spin theory (2) description of the t - J model (1) by the exchange of the spin excitation generates the d-wave charge-carrier pairing-state. The d-wave electron pairs originated from the d-wave charge-carrier pairing-state are due to charge-spin recombination⁷², and these electron pairs condensation leads to form the d-wave SC-state. The main features of the kinetic-energy-driven superconductivity can be summarized as: (i) the mechanism is purely electronic without phonons; (ii) the mechanism indicates that the strong electron correlation favors superconductivity, since the main ingredient is identified into an electron pairing mechanism not involving the phonon, the external degree of freedom, but *the spin excitation, the collective mode from the internal spin degree of freedom of the constrained electron itself*. In other words, the constrained electrons simultaneously act to glue and to be glued^{74,75}; (iii) the kinetic-energy-driven SC-state in a way is in turn strongly influenced by the single-particle coherence, which leads to that T_c takes a dome-like shape with the underdoped and overdoped regimes on each side of the optimal doping, where T_c reaches its maximum. Within the framework of the kinetic-energy-driven superconductivity, the homogeneous electron propagator of the t - J model (1) has been obtained explicitly as^{72,73},

$$G(\mathbf{k}, \omega) = \frac{1}{\omega - \varepsilon_{\mathbf{k}} - \Sigma_{\text{tot}}(\mathbf{k}, \omega)}, \quad (3a)$$

$$\mathcal{S}^\dagger(\mathbf{k}, \omega) = \frac{W(\mathbf{k}, \omega)}{\omega - \varepsilon_{\mathbf{k}} - \Sigma_{\text{tot}}(\mathbf{k}, \omega)}, \quad (3b)$$

with the electron energy dispersion in the tight-binding approximation $\varepsilon_{\mathbf{k}} = -4t\gamma_{\mathbf{k}} + 4t'\gamma'_{\mathbf{k}} + \mu$, where $\gamma_{\mathbf{k}} = (\cos k_x + \cos k_y)/2$ and $\gamma'_{\mathbf{k}} = \cos k_x \cos k_y$, and the homogeneous electron total self-energy $\Sigma_{\text{tot}}(\mathbf{k}, \omega)$ and the function $W(\mathbf{k}, \omega)$ that can be respectively expressed as,

$$\Sigma_{\text{tot}}(\mathbf{k}, \omega) = \Sigma_{\text{ph}}(\mathbf{k}, \omega) + \frac{|\Sigma_{\text{pp}}(\mathbf{k}, \omega)|^2}{\omega + \varepsilon_{\mathbf{k}} + \Sigma_{\text{ph}}(\mathbf{k}, -\omega)}, \quad (4a)$$

$$W(\mathbf{k}, \omega) = -\frac{\Sigma_{\text{pp}}(\mathbf{k}, \omega)}{\omega + \varepsilon_{\mathbf{k}} + \Sigma_{\text{ph}}(\mathbf{k}, -\omega)}, \quad (4b)$$

where $\Sigma_{\text{ph}}(\mathbf{k}, \omega)$ is the homogeneous electron normal self-energy in the particle-hole channel, and $\Sigma_{\text{pp}}(\mathbf{k}, \omega)$ is the homogeneous electron anomalous self-energy in the particle-particle channel, and have been obtained by taking into account the vertex correction as⁷³,

$$\begin{aligned} \Sigma_{\text{ph}}(\mathbf{k}, i\omega_n) &= \frac{1}{N^2} \sum_{\mathbf{p}, \mathbf{p}'} [V_{\text{ph}} \Lambda_{\mathbf{p}+\mathbf{p}'+\mathbf{k}}]^2 \\ &\times \frac{1}{\beta} \sum_{ip_m} G(\mathbf{p}+\mathbf{k}, ip_m + i\omega_n) \Pi(\mathbf{p}, \mathbf{p}', ip_m), \end{aligned} \quad (5a)$$

$$\Sigma_{pp}(\mathbf{k}, i\omega_n) = \frac{1}{N^2} \sum_{\mathbf{p}, \mathbf{p}'} [V_{pp} \Lambda_{\mathbf{p}+\mathbf{p}'+\mathbf{k}}]^2 \times \frac{1}{\beta} \sum_{ip_m} \Im^\dagger(\mathbf{p}+\mathbf{k}, ip_m + i\omega_n) \Pi(\mathbf{p}, \mathbf{p}', ip_m), \quad (5b)$$

respectively, with the bare vertex function $\Lambda_{\mathbf{k}} = 4t\gamma_{\mathbf{k}} - 4t'\gamma'_{\mathbf{k}}$. The vertex correction V_{ph} for the homogeneous electron normal self-energy, the vertex correction V_{pp} for the homogeneous electron anomalous self-energy, together with the spin bubble $\Pi(\mathbf{p}, \mathbf{p}', ip_m)$ have been derived, and are given explicitly in Ref. 73. In low-temperatures, the sharp peaks emerge in $\Sigma_{ph}(\mathbf{k}, \omega)$ and $\Sigma_{pp}(\mathbf{k}, \omega)$, which are actually δ -type functions. However, these δ -type functions are broadened by a small damping employed in the numerical calculation for a finite lattice. In this paper, the calculation for $\Sigma_{ph}(\mathbf{k}, \omega)$ and $\Sigma_{pp}(\mathbf{k}, \omega)$ is performed numerically on a 120×120 lattice in momentum space, where the infinitesimal $i0_+ \rightarrow i\Gamma$ is replaced by a small damping $\Gamma = 0.05J$.

C. Phase diagram

In the kinetic-energy-driven superconductivity^{69–73}, both the homogeneous electron normal and anomalous self-energies originate from the coupling of the electrons with the same spin excitation, however, they describe different parts of the coupling effect. The electron normal self-energy $\Sigma_{ph}(\mathbf{k}, \omega)$ describes the single-particle coherence, and its main function is to renormalize the energy and lifetime of the electrons. In particular the normal-state pseudogap is intimately related to the electron normal self-energy. To see this intimate relation more clearly, we rewrite approximately the above electron normal self-energy in Eq. (5a) as^{71–73},

$$\Sigma_{ph}(\mathbf{k}, \omega) \approx \frac{[2\bar{\Delta}_{PG}(\mathbf{k})]^2}{\omega - \varepsilon_{\mathbf{k}}}, \quad (6)$$

where $\bar{\Delta}_{PG}(\mathbf{k})$ can be derived directly as,

$$\bar{\Delta}_{PG}^2(\mathbf{k}) = -\frac{1}{4}\varepsilon_{\mathbf{k}}\Sigma_{ph}(\mathbf{k}, 0), \quad (7)$$

and is identified as being a region of the electron normal self-energy in which $\bar{\Delta}_{PG}$ anisotropically suppresses the electron density of states on EFS^{4–10}. In this sense, $\bar{\Delta}_{PG}$ can be identified as the momentum-dependent normal-state pseudogap, with the normal-state pseudogap parameter $\bar{\Delta}_{PG}^2 = (1/N)\sum_{\mathbf{k}}\bar{\Delta}_{PG}^2(\mathbf{k})$, and then all the anomalous properties of the underdoped cuprate superconductors arise from the opening of this normal-state pseudogap. However, the SC-state on the other hand is characterized by the electron anomalous self-energy $\Sigma_{pp}(\mathbf{k}, \omega)$, which is defined as the energy- and momentum-dependent electron pair gap (then the SC gap) $\Sigma_{pp}(\mathbf{k}, \omega) = \bar{\Delta}_{\mathbf{k}}(\omega)$ in the single-particle excitation spectrum, and thus is corresponding to the

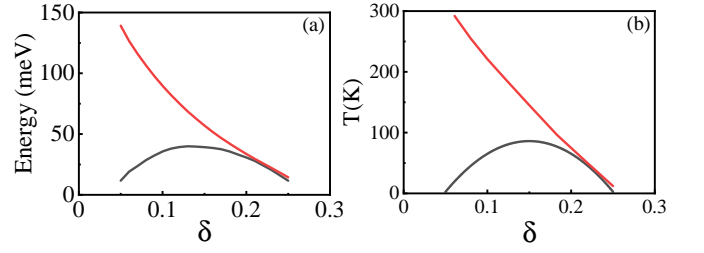


FIG. 1. (Color online) (a) The superconducting gap $2\bar{\Delta}$ (black-line) and normal-state pseudogap $2\bar{\Delta}_{PG}$ (red-line) as a function of doping with temperature $T = 0.002J$. (b) The superconducting transition temperature T_c (black-line) and the normal-state pseudogap crossover temperature T^* (red-line) as a function of doping.

energy for breaking an electron pair⁷⁶. In the static limit, this SC gap $\bar{\Delta}_{\mathbf{k}}(\omega)$ can be reduced as^{72,73},

$$\bar{\Delta}_{\mathbf{k}}(\omega) |_{\omega=0} = \bar{\Delta}_{\mathbf{k}} = \bar{\Delta}\gamma_{\mathbf{k}}^{(d)}, \quad (8)$$

with the SC gap parameter $\bar{\Delta}$ and the d-wave factor $\gamma_{\mathbf{k}}^{(d)} = (\cos k_x - \cos k_y)/2$. The above results in Eqs. (6) and (8) therefore indicate that the pseudogap-state coexists and competes with superconductivity below T_c , although the normal-state pseudogap bears no direct relation to superconductivity.

In the phase diagram of the cuprate superconductors, the crucial feature in the underdoped regime is the intertwinement of the pseudogap-state and superconductivity. To delve this intertwinement, the evolution of the pseudogap- and SC-states with doping and temperature has been investigated^{71–73}. For a better understanding of the nature of the LDOS modulation in the pseudogap phase, the results⁷³ of the SC-gap $2\bar{\Delta}$ (black-line) and normal-state pseudogap $2\bar{\Delta}_{PG}$ (red-line) as a function of doping with temperature $T = 0.002J$ are replotted in Fig. 1a, where the normal-state pseudogap and SC gap diverge in the underdoped regime, i.e., the SC gap $\bar{\Delta}$ increases smoothly with the increase of doping, and achieves its maximum at around the optimal doping $\delta \approx 0.15$, while the normal-state pseudogap $\bar{\Delta}_{PG}$ is notably larger than the SC gap $\bar{\Delta}$, and then it weakens as the optimal doping is approached^{4–11}. However, in the overdoped regime, both the normal-state pseudogap and SC gap decrease monotonically with the increase of doping, and converge to approximately same magnitude in the strongly overdoped region, eventually going to zero together at the end of the SC dome.

At a given doping concentration, the SC gap $\bar{\Delta}$ is identified with a SC transition with a SC transition temperature T_c , while the normal-state pseudogap $\bar{\Delta}_{PG}$ is defined as a crossover with a normal-state pseudogap crossover temperature T^* . To see this doping dependence of T_c and T^* more directly, the results⁷³ of T_c (black-line) and T^* (red-line) as a function of doping are replotted in Fig. 1b, where in conformity with the doping dependence of $\bar{\Delta}$ and $\bar{\Delta}_{PG}$ shown in Fig. 1a, (i) T_c is

raised monotonically upon the increase of doping in the underdoped regime, and achieves its maximum at around the optimal doping, then T_c turns into a gradual decrease in the overdoped regime; (ii) the pseudogap-state in the underdoped regime exhibits a pseudogap at temperature T^* large compared to T_c , and then this T^* decreases with the increase of doping, as opposed to T_c . However, T^* seems to degenerate with T_c in the strongly overdoped region, and goes approximately to zero together with T_c at the end of the SC dome^{4–11}. This T^* is actually a crossover temperature below which a novel electronic state emerges, where the distinguished features are characterized by the presence of the Fermi arcs^{77–81}, the static and fluctuating ordering phenomena^{43–48}, the dramatic change in the line-shape of the energy distribution curve^{48–56}, and the kink in the quasiparticle dispersion^{57–62}, etc., and are correlated directly to the opening of the normal-state pseudogap^{4–10}.

D. Reconstruction of constant energy contour

The essential feature of the low-energy quasiparticle excitation detected from ARPES experiments can be analyzed theoretically in terms of the ARPES spectral intensity^{6–8},

$$I(\mathbf{k}, \omega) \propto n_F(\omega) A(\mathbf{k}, \omega), \quad (9)$$

where $n_F(\omega)$ is the fermion distribution, while the electron spectral function $A(\mathbf{k}, \omega)$ is related directly with the imaginary part of the homogeneous electron diagonal propagator (3a) as,

$$\begin{aligned} A(\mathbf{k}, \omega) &= -\frac{1}{\pi} \text{Im} G(\mathbf{k}, \omega) \\ &= \frac{1}{\pi} \frac{\tilde{\Gamma}_{\mathbf{k}}(\omega)}{[\omega - \varpi_{\mathbf{k}}(\omega)]^2 + [\tilde{\Gamma}_{\mathbf{k}}(\omega)]^2}, \end{aligned} \quad (10)$$

with the quasiparticle energy dispersion and quasiparticle scattering rate,

$$\varpi_{\mathbf{k}}(\omega) = \varepsilon_{\mathbf{k}} - \text{Re}\Sigma_{\text{tot}}(\mathbf{k}, \omega), \quad (11a)$$

$$\tilde{\Gamma}_{\mathbf{k}}(\omega) = \text{Im}\Sigma_{\text{tot}}(\mathbf{k}, \omega), \quad (11b)$$

in the SC-state, respectively, where $\text{Re}\Sigma_{\text{tot}}(\mathbf{k}, \omega)$ and $\text{Im}\Sigma_{\text{tot}}(\mathbf{k}, \omega)$ are the real and imaginary parts of the homogeneous electron total self-energy $\Sigma_{\text{tot}}(\mathbf{k}, \omega)$. In particular, when the SC gap parameter $\tilde{\Delta} = 0$ in the pseudogap phase above T_c , these quasiparticle energy dispersion and quasiparticle scattering rate in Eq. (11) in the SC-state are reduced as,

$$\varpi_{\mathbf{k}}(\omega) = \varepsilon_{\mathbf{k}} - \text{Re}\Sigma_{\text{ph}}(\mathbf{k}, \omega), \quad (12a)$$

$$\tilde{\Gamma}_{\mathbf{k}}(\omega) = \text{Im}\Sigma_{\text{ph}}(\mathbf{k}, \omega) \approx \pi[2\tilde{\Delta}_{\text{PG}}(\mathbf{k})]^2 \delta(\omega - \varepsilon_{\mathbf{k}}), \quad (12b)$$

in the pseudogap phase, respectively, with the real part $\text{Re}\Sigma_{\text{ph}}(\mathbf{k}, \omega)$ and the imaginary part $\text{Im}\Sigma_{\text{ph}}(\mathbf{k}, \omega)$ of the

homogeneous electron normal self-energy, respectively. The above results in Eqs. (11b) and (12b) therefore show clearly whether in the SC-state or in the normal-state, the quasiparticle scattering rate is intrinsically correlated to the normal-state pseudogap, which is consistent with the experimental observations⁸².

In the previous discussions, both the experimental observations^{37–42} and theoretical studies^{22,83,84} indicate that in the underdoped regime, the constant energy contour in the SC-state at the case for a finite binding-energy is truncated into the Fermi arcs centered at around the nodal region, where the notation *Fermi arcs* on the constant energy contour has been used even for a finite binding-energy. Moreover, these experimental observations and theoretical studies also show that the Fermi arcs are not strongly peaked intensities at around the nodes, however, the highest intensities are located at around the tips of the Fermi arcs. These tips of the Fermi arcs connected by the scattering wave vectors \mathbf{q}_i then construct an *octet scattering model*^{37–42}, which is a basic scattering model for the interpretation of the SC-state QSI in cuprate superconductors^{19–29}. Since the SC- and pseudogap-states coexist below T_c and the quasiparticle scattering rate is proportional to the normal-state pseudogap, it has been thus shown that the formation of the Fermi arcs and the related octet scattering model due to the redistribution of the spectral weight on the constant energy contour for a finite binding-energy is directly linked with the opening of the highly anisotropic momentum-dependence of the normal-state pseudogap.

Very recently, we⁷³ have studied the exotic features of the low-energy electronic structure of cuprate superconductors in the pseudogap phase, where we found that the characteristic of the octet scattering model in the SC-state remain unchanged upon passing above T_c to the pseudogap phase, in agreement with the experimental observations^{37–42}. For a convenience in the following discussion of the LDOS modulation in the pseudogap phase, the constant energy contours in the $[k_x, k_y]$ plane at doping $\delta = 0.09$ for the binding-energy $\omega = 0.06J$ in (a) the pseudogap phase with temperature $T = 0.07J$ and (b) the SC-state with temperature $T = 0.002J$ are replotted in Fig. 2. Expectedly, as in the case of the SC-state^{22,83,84}, (i) the structure of the constant energy contour intensity maps and the dispersions of the seven scattering wave vectors $\mathbf{q}_i(\omega)$ [$i = 1, 2, \dots, 7$] are essentially the same both in the SC-state and pseudogap phase. In particular, the tips of the Fermi arcs connected by the scattering wave vectors $\mathbf{q}_i(\omega)$ in the pseudogap phase still construct an *octet scattering model*; (ii) all seven scattering wave vectors $\mathbf{q}_i(\omega)$ retain their particle-hole symmetry $\mathbf{q}_i(\omega) = \mathbf{q}_i(-\omega)$ in the pseudogap phase, then the LDOS modulations occur in the same energy range, and emanate from the same constant energy contour in momentum-space as those observed in the SC-state. However, there is a substantial difference between the pseudogap phase and SC-state at around

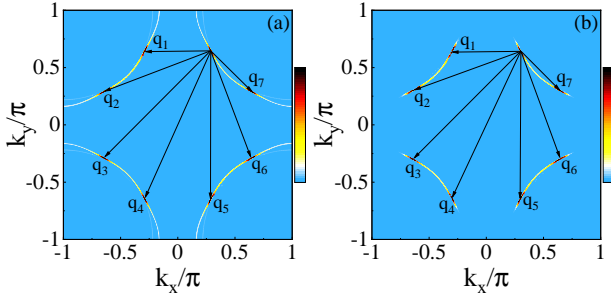


FIG. 2. (Color online) The constant energy contour map in the $[k_x, k_y]$ plane at doping $\delta = 0.09$ for the binding-energy $\omega = 0.06J$ in (a) the pseudogap phase with temperature $T = 0.07J$ and (b) the superconducting-state with temperature $T = 0.002J$. The eight tips of the Fermi arcs determine the scattering within the octet scattering model, while the scattering wave vectors which connect the tips of the Fermi arcs are shown as arrows labeled by the designation of each scattering wave vector \mathbf{q}_i .

the antinodal region, namely, the spectral weight at around the antinodal region in the SC-state is gapped out completely by both the SC gap and normal-state pseudogap, while the spectral weight at around the antinodal region in the pseudogap phase is suppressed partially by the normal-state pseudogap only, which leads to that small residual spectral-weight exists at around the antinodal region in the pseudogap phase. This small residual spectral-weight may induce the unusual charge ordering in the pseudogap phase, and we will discuss this issue towards in Sec. IV.

III. LOCAL DENSITY OF STATES

A. Local density of states in superconducting-state

In the recent work⁶³, LDOS in the SC-state has been derived for various kinds of impurities. For the discussion of the LDOS modulation in the pseudogap phase and then comparison it with the LDOS modulation in the SC-state, here the main formalism of LDOS in the SC-state and the related T -matrix are summarized briefly. In the presence of impurities with the impurity-scattering potential $V(\mathbf{r})$, the homogeneous electron propagator (3) in the SC-state is dressed by the impurity scattering, while this dressed electron propagator has been obtained within the T -matrix approach as⁶³,

$$\tilde{G}_I(\mathbf{k}, \mathbf{k}', \omega) = \tilde{G}(\mathbf{k}, \omega) \delta_{\mathbf{k}, \mathbf{k}'} + \tilde{G}(\mathbf{k}, \omega) \tilde{T}_{\mathbf{k}\mathbf{k}'}(\omega) \tilde{G}(\mathbf{k}', \omega), \quad (13)$$

where $\tilde{G}(\mathbf{k}, \omega)$ is the homogeneous electron propagator (3) in the Nambu representation, and the T -matrix $\tilde{T}_{\mathbf{k}\mathbf{k}'}(\omega)$ satisfies the following iteration equation,

$$\tilde{T}_{\mathbf{k}\mathbf{k}'}(\omega) = \frac{1}{N} V_{\mathbf{k}\mathbf{k}'} \tau_3 + \frac{1}{N} \sum_{\mathbf{k}_2} V_{\mathbf{k}\mathbf{k}_2} \tau_3 \tilde{G}(\mathbf{k}_2, \omega) \tilde{T}_{\mathbf{k}_2\mathbf{k}'}(\omega), \quad (14)$$

with the impurity-scattering potential in momentum-space,

$$V_{\mathbf{k}_1\mathbf{k}_2} = V(\mathbf{k}_1 - \mathbf{k}_2) = \sum_{\mathbf{r}} e^{-i(\mathbf{k}_1 - \mathbf{k}_2) \cdot \mathbf{r}} V(\mathbf{r}). \quad (15)$$

In this case, the corresponding form of the dressed electron propagator in real-space can be derived directly in terms of the Fourier transform as,

$$\begin{aligned} \tilde{G}_I(\mathbf{r}, \mathbf{r}', \omega) &= \tilde{G}(\mathbf{r} - \mathbf{r}', \omega) \\ &+ \frac{1}{N} \sum_{\mathbf{k}, \mathbf{k}'} e^{i\mathbf{k} \cdot \mathbf{r} - i\mathbf{k}' \cdot \mathbf{r}'} \tilde{G}(\mathbf{k}, \omega) \tilde{T}_{\mathbf{k}\mathbf{k}'}(\omega) \tilde{G}(\mathbf{k}', \omega). \end{aligned} \quad (16)$$

The above results in Eqs. (13) and (16) thus indicate unambiguously that the nature of the LDOS modulation is governed by both the homogeneous electron propagator (then the constant energy contour and the related octet scattering model), which reflects the effect of the strong electron correlation on the LDOS modulation, and the impurity-generated T -matrix, which incorporates both the effects of the strong electron correlation and impurity-scattering on the LDOS modulation. The above results in Eqs. (13) and (16) also show that in addition to the homogeneous electron propagator, the more accurate result of the T -matrix should be obtained in the proper discussion of the LDOS modulation. In this case, we⁶³ have developed a powerful method of the inversion of matrix, and then the above impurity-generated T -matrix in Eq. (14) has been derived accurately as,

$$\tilde{T}(\omega) = \bar{V} \otimes \tau_0 \frac{1}{1 - \bar{M}} \hat{I}_v \otimes \tau_3, \quad (17)$$

with a unit matrix in momentum-space \hat{I}_v , and the matrices \bar{V} and \bar{M} that have been given explicitly in Ref. 63. It should be emphasized that in this approach of the inversion of matrix, the derivation of the T -matrix consists of all the quasiparticle excitations and scattering processes.

The real-space LDOS modulation $\delta\rho(\mathbf{r}, \omega)$ now can be evaluated directly from the imaginary part of the diagonal matrix elements of the impurity-dressed electron propagator (16) as,

$$\begin{aligned} \delta\rho(\mathbf{r}, \omega) &= \rho(\mathbf{r}, \omega) - \rho_0(\omega) \\ &= -\frac{2}{\pi} \text{Im} \left[\frac{1}{N} \sum_{\mathbf{k}\mathbf{k}'} e^{i(\mathbf{k} - \mathbf{k}') \cdot \mathbf{r}} \tilde{G}(\mathbf{k}, \omega) \tilde{T}_{\mathbf{k}\mathbf{k}'}(\omega) \tilde{G}(\mathbf{k}', \omega) \right]_{11}, \end{aligned} \quad (18)$$

with the density of states in the case of the absence of impurities $\rho_0(\omega)$. The momentum-space LDOS modulation $\delta\rho(\mathbf{q}, \omega)$ is easily obtained from the above real-space LDOS modulation $\delta\rho(\mathbf{r}, \omega)$ in Eq. (18) by using the Fourier-transform as,

$$\delta\rho(\mathbf{q}, \omega) = \text{Re}[\delta\rho(\mathbf{q}, \omega)] + i\text{Im}[\delta\rho(\mathbf{q}, \omega)], \quad (19)$$

where $\text{Re}[\delta\rho(\mathbf{q}, \omega)]$ and $\text{Im}[\delta\rho(\mathbf{q}, \omega)]$ are respectively the corresponding real and imaginary parts of the LDOS

modulation $\delta\rho(\mathbf{q}, \omega)$, and can be expressed explicitly as,

$$\text{Re}[\delta\rho(\mathbf{q}, \omega)] = -\frac{1}{\pi}\text{Im}[\tilde{A}_I(\mathbf{q}, \omega) + \tilde{A}_I(-\mathbf{q}, \omega)]_{11}, \quad (20a)$$

$$\text{Im}[\delta\rho(\mathbf{q}, \omega)] = -\frac{1}{\pi}\text{Re}[\tilde{A}_I(\mathbf{q}, \omega) - \tilde{A}_I(-\mathbf{q}, \omega)]_{11}, \quad (20b)$$

with the related spectral function,

$$\tilde{A}_I(\mathbf{q}, \omega) = \sum_{\mathbf{k}} \tilde{G}(\mathbf{k}, \omega) \tilde{T}(\mathbf{k}, \mathbf{k} + \mathbf{q}, \omega) \tilde{G}(\mathbf{k} + \mathbf{q}, \omega). \quad (21)$$

B. Local density of states in pseudogap phase

In the pseudogap phase, where the SC gap $\bar{\Delta} = 0$, the homogeneous electron propagator (3) in the SC-state is reduced as,

$$G(\mathbf{k}, \omega) = \frac{1}{\omega - \varepsilon_{\mathbf{k}} - \Sigma_{\text{ph}}(\mathbf{k}, \omega)}, \quad (22)$$

and then the impurity-dressed electron propagator (13) in the SC-state and the related T -matrix iteration equation (14) are respectively reduced as,

$$G_I(\mathbf{k}, \mathbf{k}', \omega) = G(\mathbf{k}, \omega) \delta_{\mathbf{k}, \mathbf{k}'} + G(\mathbf{k}, \omega) T_{\mathbf{k}\mathbf{k}'}(\omega) G(\mathbf{k}', \omega), \quad (23a)$$

$$T_{\mathbf{k}\mathbf{k}'}(\omega) = \bar{V}_{\mathbf{k}\mathbf{k}'} + \sum_{\mathbf{k}_1} \bar{V}_{\mathbf{k}\mathbf{k}_1} G(\mathbf{k}_1, \omega) T_{\mathbf{k}_1\mathbf{k}'}(\omega). \quad (23b)$$

As in the case of the SC-state T -matrix (17) mentioned in the above subsection III A, the T -matrix in the pseudogap phase can be also derived accurately by making use of the approach of the inversion of matrix as [see Appendix A],

$$T(\omega) = \bar{V} \frac{1}{1 - \bar{M}}. \quad (24)$$

With the help of the Fourier-transform, the impurity-dressed electron propagator $G_I(\mathbf{r}, \mathbf{r}', \omega)$ in real-space now can be derived straightforwardly from the impurity-dressed electron propagator $G_I(\mathbf{k}, \mathbf{k}', \omega)$ in Eq. (23a) in momentum-space as,

$$G_I(\mathbf{r}, \mathbf{r}', \omega) = G(\mathbf{r} - \mathbf{r}', \omega) + \frac{1}{N} \sum_{\mathbf{k}, \mathbf{k}'} e^{i\mathbf{k} \cdot \mathbf{r} - i\mathbf{k}' \cdot \mathbf{r}'} G(\mathbf{k}, \omega) \times T_{\mathbf{k}\mathbf{k}'}(\omega) G(\mathbf{k}', \omega), \quad (25)$$

and then the real-space LDOS modulation $\delta\rho(\mathbf{r}, \omega)$ can be obtain from the imaginary part of the above impurity-dressed electron propagator (25) as,

$$\delta\rho(\mathbf{r}, \omega) = -\frac{1}{\pi} \text{Im} \left[\frac{1}{N} \sum_{\mathbf{k}, \mathbf{k}'} e^{i(\mathbf{k} - \mathbf{k}') \cdot \mathbf{r}} G(\mathbf{k}, \omega) \times T_{\mathbf{k}\mathbf{k}'}(\omega) G(\mathbf{k}', \omega) \right]. \quad (26)$$

In this case, the corresponding momentum-space LDOS modulation $\delta\rho(\mathbf{q}, \omega)$ can be evaluated directly from the above real-space LDOS modulation $\delta\rho(\mathbf{r}, \omega)$ in terms of the Fourier-transform as,

$$\delta\rho(\mathbf{q}, \omega) = \text{Re}\delta\rho(\mathbf{q}, \omega) + i\text{Im}\delta\rho(\mathbf{q}, \omega), \quad (27)$$

where $\text{Re}\delta\rho(\mathbf{q}, \omega)$ and $\text{Im}\delta\rho(\mathbf{q}, \omega)$ are given as,

$$\text{Re}\delta\rho(\mathbf{q}, \omega) = -\frac{1}{\pi} \text{Im}[A_I(\mathbf{q}, \omega) + A_I(-\mathbf{q}, \omega)], \quad (28a)$$

$$\text{Im}\delta\rho(\mathbf{q}, \omega) = -\frac{1}{\pi} \text{Re}[A_I(\mathbf{q}, \omega) - A_I(-\mathbf{q}, \omega)], \quad (28b)$$

respectively, with the related spectral function,

$$A_I(\mathbf{q}, \omega) = \sum_{\mathbf{k}} G(\mathbf{k}, \omega) T(\mathbf{k}, \mathbf{k} + \mathbf{q}, \omega) G(\mathbf{k} + \mathbf{q}, \omega). \quad (29)$$

According to the above real and imaginary parts of the momentum-space LDOS modulation in Eq. (28), the weight $|\delta\rho(\mathbf{q}, \omega)|$ and the phase $\phi(\mathbf{q}, \omega)$ of the LDOS modulation spectrum are obtained explicitly as,

$$|\delta\rho(\mathbf{q}, \omega)| = \sqrt{\text{Re}\delta\rho(\mathbf{q}, \omega)^2 + \text{Im}\delta\rho(\mathbf{q}, \omega)^2}, \quad (30a)$$

$$\phi(\mathbf{q}, \omega) = \arctan \left(\frac{\text{Im}\delta\rho(\mathbf{q}, \omega)}{\text{Re}\delta\rho(\mathbf{q}, \omega)} \right) + \pi\theta(-\text{Re}\delta\rho(\mathbf{q}, \omega)), \quad (30b)$$

respectively. The characteristic feature in the momentum-space LDOS modulation spectrum $\delta\rho(\mathbf{q}, \omega)$ is governed by the peaks^{30–36}, while the peaks for a given energy ω is corresponding to the momentum-space highest joint density of states at that energy ω , and then $\mathbf{q}(\omega)$ of the peaks in the LDOS modulation spectrum can be straightforwardly connected to the quasiparticle dispersion.

IV. QUANTITATIVE CHARACTERISTICS

In this section, we discuss the quantitative characteristics of the LDOS modulation in the underdoped cuprate superconductors generated by various kinds of a single impurity to shed light on the nature of the quasiparticle excitation in the pseudogap phase and of its similarity and difference with the corresponding one in the SC-state. As in our recent studies⁶³, the strength of the impurity scattering potential in the following discussion is set to be positive to refrain from the quantum resonant state, since the T -matrix approach is not valid for the case of the quantum resonant state generated by the impurity scattering potential with the negative strength.

The crystal structure of cuprate superconductors is a stacking of the common CuO_2 planes separated by insulating layers^{14,15}, the impurity distribution accompanied with different types of the doping processes are quite different^{16–18}. In particular, impurities which

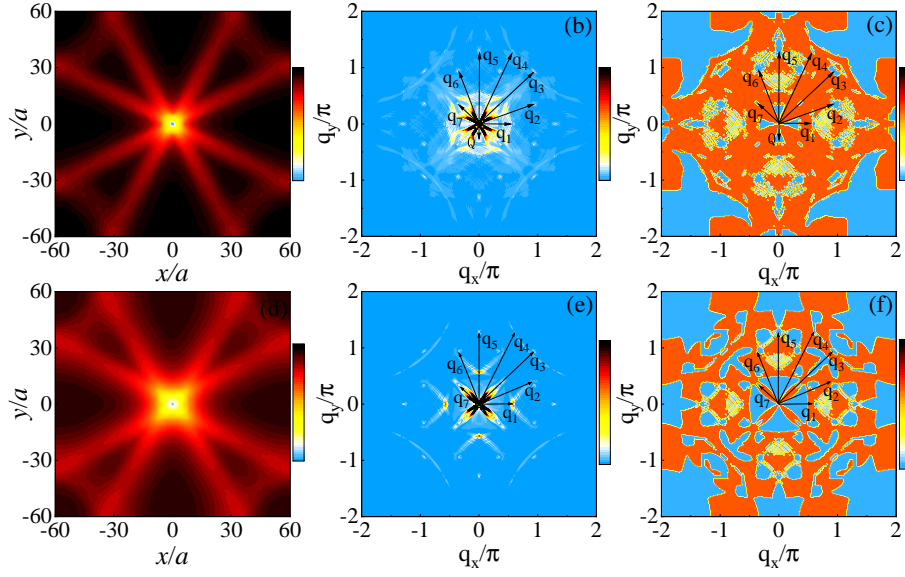


FIG. 3. (Color online) Upper panel: the intensity maps of (a) the local density of states in real-space, (b) the amplitude of the local density of states in momentum-space, and (c) the phase of the momentum-space local density of states in the pseudogap phase for an in-plane single impurity at doping $\delta = 0.09$ and the binding-energy $\omega = 0.06J$ with temperature $T = 0.07J$ for the impurity-scattering strength $V_s = 1.0J$ and screening length $L = 5.0a$. Lower panel: the corresponding intensity maps of (d) the local density of states in real-space, (e) the amplitude of the local density of states in momentum-space, and (f) the phase of the momentum-space local density of states in the superconducting-state with temperature $T = 0.002J$.

substitute for Cu in the CuO_2 plane turn out to be strong scatterers of the electronic state in the CuO_2 plane, giving rise to a major modification of the electronic structure. The impurity-scattering potential for an in-plane single impurity located at the lattice site $\mathbf{r} = 0$ can be modeled in real-space by a screened Coulomb potential with the screening length as^{16–18},

$$V(\mathbf{r}) = \frac{V_s}{|\mathbf{r}|} e^{-|\mathbf{r}|/L}, \quad (31)$$

where V_s is the in-plane impurity-scattering strength, L is the screening length, while its Fourier-transformed form can be derived straightforwardly as,

$$V_{\mathbf{k}\mathbf{k}'} = \frac{2\pi V_s}{\sqrt{(\mathbf{k} - \mathbf{k}')^2 + 1/L^2}}. \quad (32)$$

In the following discussion, the in-plane impurity-scattering strength V_s and its screening length L are chosen as $V_s = 1.0J$ and $L = 5.0a$, respectively.

To characterize the LDOS modulation in the pseudogap phase, we have performed a series of calculations for LDOS both in real- and momentum-spaces for an in-plane single impurity in the *pseudogap phase*, and the obtained results of the intensity maps of (a) the LDOS modulation in real-space, (b) the amplitude of the LDOS modulation in momentum-space, and (c) the phase of the momentum-space LDOS modulation at doping $\delta = 0.09$ and the binding-energy $\omega = 0.06J$ with temperature $T = 0.07J$ for the impurity-scattering strength $V_s = 1.0J$ and screening length $L =$

$5.0a$ are plotted in the upper panel of Fig. 3. For a clear comparison, the corresponding results⁶³ of the intensity maps of (d) the LDOS modulation in real-space, (e) the amplitude of the LDOS modulation in momentum-space, and (f) the phase of the momentum-space LDOS modulation in the SC-state with temperature $T = 0.002J$ are replotted in the lower panel of Fig. 3. The main features of the obtained results can be summarized as:

- (i) The global feature of the real-space LDOS modulation in the pseudogap phase is similar to that in the SC-state (see Fig. 3a and Fig. 3d), i.e., the real-space LDOS modulation in the pseudogap phase presents a similar ripple pattern as that in the SC-state. However, the weight of the LDOS modulation in momentum-space centered at around the nodal region is effectively reduced in the pseudogap phase, which in turn weakens the LDOS modulation in real-space along the diagonal direction, leading to that the intensity of the ripples is decreased, and the weight of the LDOS modulation connected two ripples along the diagonal direction vanishes in the pseudogap phase. Furthermore, the fuzzy region in the momentum-space LDOS modulation pattern with small momenta along the antinodal direction appears in the pseudogap phase, while the small weight in this fuzzy region in the pseudogap phase is suppressed strongly in the SC-state by the SC gap, leading to a more clearer SC-state QSI pattern in the momentum-space LDOS modulation;
- (ii) The SC-state QSI peaks in the momentum-space LDOS modulation are located exactly at the discrete spots⁶³ (see Fig. 3e), where these discrete spots

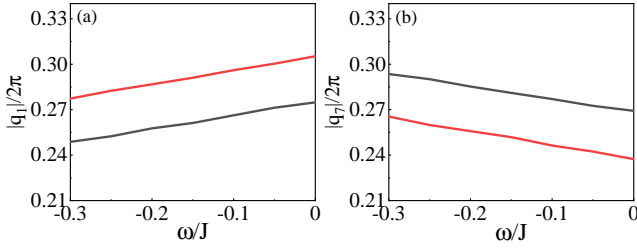


FIG. 4. (Color online) The evolution of the scattering wave vectors (a) \mathbf{q}_1 and (b) \mathbf{q}_7 with energy in the pseudogap phase for an in-plane single impurity at doping $\delta = 0.09$ (red-line) and doping $\delta = 0.12$ (black-line) with temperature $T = 0.07J$ for the impurity-scattering strength $V_s = 1.0J$ and screening length $L = 5.0a$.

identified as regions of the high joint density of states are accommodated at around the scattering wave vectors \mathbf{q}_i with $i = 1, 2, \dots, 7$ obeying the *octet scattering model* shown in Fig. 2b. Moreover, all these QSI signatures detectable in the SC-state survive virtually unchanged into the pseudogap phase (see Fig. 3b), i.e., the QSI octet phenomenology in the SC-state^{24–29} exists in the pseudogap phase^{30–36}, then the multiple ordered electronic-states, which emerge in the pseudogap phase above T_c , persist into the SC-state below T_c and coexist and compete with the SC-state. As a natural consequence, all seven scattering wave vectors $\mathbf{q}_i(\omega)$, which are dispersive in the SC-state, remain dispersive into the pseudogap phase. To characterize typical QSI peak dispersions in the pseudogap phase more clearly, we plot the energy dependence of the QSI peaks in the pseudogap phase for the scattering wave vectors (a) \mathbf{q}_1 and (b) \mathbf{q}_7 at doping $\delta = 0.09$ (red-line) and doping $\delta = 0.12$ (black-line) with temperature $T = 0.07J$ for an in-plane single impurity for the impurity-scattering strength $V_s = 1.0J$ and screening length $L = 5.0a$ in Fig. 4, where for a given doping concentration, the peak at the scattering wave vector \mathbf{q}_1 evolves very differently with energy than the peak at the scattering wave vector \mathbf{q}_7 , and their dispersions have opposite sign, i.e., the length of \mathbf{q}_1 becomes shorter, whereas the length of \mathbf{q}_7 becomes longer, as energy $|\omega|$ is increased. However, with the increase of the doping concentration, \mathbf{q}_1 decreases systematically in length, while \mathbf{q}_7 moves to higher values, which are expected since the distance between the parallel tips of the Fermi arcs moves closer together, while the distance between the diagonal tips of the Fermi arcs increases^{22,83}. The results of the evolution of the QSI peaks with energy and doping in Fig. 4 therefore further confirm that as in the case of the SC-state^{24–29}, the typical QSI peak dispersions in the pseudogap phase are also internally consistent within the octet scattering model shown in Fig. 2a. These results in Fig. 3 and Fig. 4 are also in qualitative agreement with the STM/S^{30–36} and ARPES^{41,42,85} experimental observations, where the doping and energy dependence of the positions of the tips of the Fermi arcs (then the scattering wave vectors \mathbf{q}_i) in

the pseudogap phase have been observed. In particular, the ARPES experiments^{43–48} have indicated clearly that in the pseudogap phase, the magnitude of the charge-order wave vector $Q_{co} = \mathbf{q}_1$ smoothly decreases with the increase of doping, which is also in agreement with the present result shown in Fig. 4.

(iii) As in the case of the SC-state⁶³ (see Fig. 3f), the phase $\phi(\mathbf{q}, \omega)$ of the momentum-space LDOS modulation pattern in the pseudogap phase also exhibits a non-zero phase factor of π centered at around $\mathbf{q} = \mathbf{0}$ along the diagonal direction (see Fig. 3c), where the most coherent quasiparticles are located. However, in correspondence with the spectral weight distribution of the coherent LDOS modulation spectrum in momentum-space, the phase $\phi(\mathbf{q}, \omega)$ in the SC-state exhibits a far more coherent behavior than that in the pseudogap phase;

(iv) However, in addition to the above QSI octet phenomenology, the exotic electronic excitation in the pseudogap phase exhibits the LDOS modulation peaks in momentum-space that are oriented along the parallel direction at the finite scattering wave vectors $\mathbf{Q} \approx [\pm 0.36\pi, 0]$ and $\mathbf{Q} \approx [0, \pm 0.36\pi]$. Among the charge-order states observed in the experiments, the period of the LDOS modulation obtained in the present work at the charge-order wave vector \mathbf{Q} corresponds most closely to that the expected checkerboard charge ordering, which is commonly observed in STM/S³⁰ and the ARPES⁸⁵ measurements on cuprate superconductors in the pseudogap phase. In the early STM/S³⁰ and ARPES⁸⁵ experiments, the *checkerboard charge ordering* was detected in the pseudogap phase above T_c . Latter, some STM/S experimental measurements^{31–36} indicated that although the checkerboard charge ordering appeared in the pseudogap phase can persist into the SC-state below T_c , the magnitude of the incoming photon energy in these experiments is larger than that of the SC gap ($|\omega| > \bar{\Delta}$). However, whether the checkerboard charge ordering observed in the pseudogap phase or in the SC-state with the magnitude of the incoming photon energy large compared to the SC gap^{30–36,85}, the average values of the checkerboard charge-order wave vectors have been identified in these experiments as $\mathbf{Q} \approx [\pm 0.44\pi, 0] \pm 15\%$ and $\mathbf{Q} \approx [0, \pm 0.44\pi] \pm 15\%$, which are qualitatively consistent with the present results. The checkerboard charge-order state is characterized by the checkerboard charge-order wave vector \mathbf{Q} , and the qualitative agreement between theory and experiments in the checkerboard charge-order wave vector therefore is important to confirm that the checkerboard charge-order state is generated by the opening of the normal-state pseudogap. More specially, this checkerboard charge ordering is a static electronic order. To see this unusual feature more clearly, we have also made a series of calculations for the magnitude of the checkerboard charge-order wave vector $|\mathbf{Q}|$ at different energies, and the result of $|\mathbf{Q}|$ as a function of energy for an in-plane single impurity at doping $\delta = 0.09$ with temperature $T = 0.07J$ for the impurity-scattering strength $V_s = 1.0J$

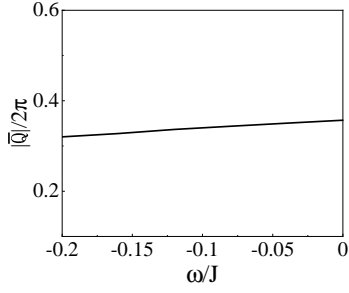


FIG. 5. The magnitude of the checkerboard charge-order wave vector as a function of energy for an in-plane single impurity at doping $\delta = 0.09$ with temperature $T = 0.07J$ for the impurity-scattering strength $V_s = 1.0J$ and screening length $L = 5.0a$.

and screening length $L = 5.0a$ is plotted in Fig. 5, where $|\mathbf{Q}|$ is almost independent on energy, confirming that this checkerboard charge ordering is non-dispersive, also in qualitative agreement with the experimental observations^{30–36,85}.

However, in STM/S experiments, the severe systematic error in the direct measurement of LDOS is produced due to tip elevation errors^{19–21}, which leads to fuzz the LDOS modulation pattern in real-space, and broaden the LDOS modulation peaks in momentum-space. In this case, it is possible that some intrinsic aspects of the the quasiparticle excitation in cuprate superconductors may be masked by the direct measurement of LDOS. Fortunately, with the improvements in the resolution of STM/S experiments^{27,86,87}, the severe systematic error in the direct measurement of LDOS can be cancelled effectively by the measurement of the ratio of differential conductances at opposite bias,

$$Z(\mathbf{r}, V) \equiv g(\mathbf{r}, +V)/g(\mathbf{r}, -V), \quad (33)$$

yet retains all the quasiparticle excitation information in the differential conductance, where V is the bias voltage, and $g(\mathbf{r}, V)$ is the differential conductance. This differential conductance $g(\mathbf{r}, \omega)$ is closely related to the LDOS $\rho(\mathbf{r}, \omega)$, and then the intrinsic features of the ratio of differential conductances at opposite bias can be analyzed theoretically in terms of LDOS,

$$Z(\mathbf{r}, \omega) = \frac{\rho(\mathbf{r}, \omega)}{\rho(\mathbf{r}, -\omega)}. \quad (34)$$

Since the condition $\rho_0(\omega) \gg \delta\rho(\mathbf{r}, \omega)$ is well satisfied for cuprate superconductors, the ratio of LDOS at opposite energy (34) can be obtained approximately by the LDOS modulation $\delta\rho(\mathbf{r}, \omega)$ as⁸⁸,

$$Z(\mathbf{r}, \omega) \approx Z_0(\omega) \left[1 + \frac{\delta\rho(\mathbf{r}, \omega)}{\rho_0(\omega)} - \frac{\delta\rho(\mathbf{r}, -\omega)}{\rho_0(-\omega)} \right], \quad (35)$$

where $Z_0(\omega) = \rho_0(\omega)/\rho_0(-\omega)$, and only the first-order modulation $\delta\rho(\mathbf{r}, \pm\omega)$ is kept. In this case, the

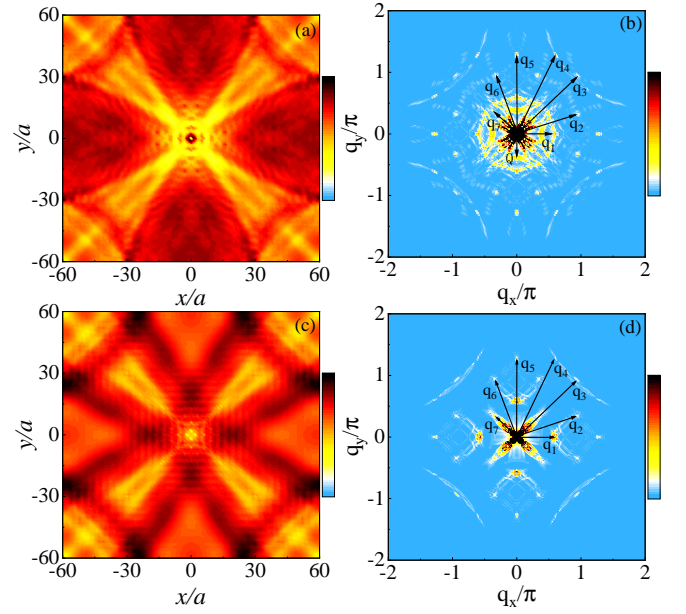


FIG. 6. (Color online) Upper panel: the intensity maps of the ratio of the local density of states at opposite energy in the pseudogap phase for an in-plane single impurity in (a) real-space and (b) momentum-space at doping $\delta = 0.09$ with temperature $T = 0.07J$ in the binding-energy $\omega = 0.06J$ for the impurity-scattering strength $V_s = 1.0J$ and screening length $L = 5.0a$. Lower panel: the corresponding intensity maps of the ratio of the local density of states at opposite energy in the superconducting-state for an in-plane single impurity in (c) real-space and (d) momentum-space with temperature $T = 0.002J$.

modulation of the ratio of the LDOS at opposite energy can be expressed explicitly as,

$$\begin{aligned} \delta Z(\mathbf{r}, \omega) &= Z(\mathbf{r}, \omega) - Z_0(\omega) \\ &\approx Z_0(\omega) \left[\frac{\delta\rho(\mathbf{r}, \omega)}{\rho_0(\omega)} - \frac{\delta\rho(\mathbf{r}, -\omega)}{\rho_0(-\omega)} \right], \end{aligned} \quad (36)$$

and its form in momentum-space then is derived straightforwardly by using the Fourier transformation as,

$$\delta Z(\mathbf{q}, \omega) \approx Z_0(\omega) \left[\frac{\delta\rho(\mathbf{q}, \omega)}{\rho_0(\omega)} - \frac{\delta\rho(\mathbf{q}, -\omega)}{\rho_0(-\omega)} \right]. \quad (37)$$

Consequently, this $\delta Z(\mathbf{q}, \omega)$ analysis can help to enhance and unmask minute details of the quasiparticle excitation free from any set-point-related issues.

To show the unmasked minute details of the quasiparticle excitation more clearly, we plot the intensity maps of the ratio of the LDOS at opposite energy in the pseudogap phase in (a) real-space and (b) momentum-space at doping $\delta = 0.09$ with temperature $T = 0.07J$ in the binding-energy $\omega = 0.06J$ for the impurity-scattering strength $V_s = 1.0J$ and screening length $L = 5.0a$ in the upper panel of Fig. 6, while the corresponding intensity maps of the ratio of LDOS at opposite energy in the SC-state in (c)

real-space and (d) momentum-space with temperature $T = 0.002J$ are plotted in the lower panel of Fig. 6, where the overall features of the δZ modulation are quite similar to the corresponding results of the LDOS modulations shown in Fig. 3, however, there are some substantial differences between the δZ modulation and LDOS modulation: (i) the intensity of the real-space LDOS modulation along the diagonal direction in Fig. 3 is enhanced in the $\delta Z(\mathbf{r}, \omega)$ modulation both in the pseudogap phase and SC-state, leading to that two ripples observed on the LDOS modulation along the diagonal direction in Fig. 3 are converted into a region in the $\delta Z(\mathbf{r}, \omega)$ modulation. In particular, the vanished weight of the LDOS modulation connected two ripples along the diagonal direction in the pseudogap phase shown in Fig. 3a is recovered in the $\delta Z(\mathbf{r}, \omega)$ modulation; (ii) the intensity of the momentum-space QSI peaks appeared in the LDOS modulation both in the pseudogap phase and SC-state is enhanced in the $\delta Z(\mathbf{q}, \omega)$ modulation, and then the QSI peaks becomes more sharper in the $\delta Z(\mathbf{q}, \omega)$ modulation; (iii) more importantly, in the pseudogap phase, the intensity of the momentum-space checkerboard peaks emerged in the LDOS modulation in Fig. 3b is strongly enhanced in the $\delta Z(\mathbf{q}, \omega)$ modulation, and then the fuzziness around checkerboard peaks in the LDOS modulation is eliminated, leading to that the more sharper and clearer checkerboard peaks appear in the $\delta Z(\mathbf{q}, \omega)$ modulation. The above results are qualitatively consistent with the corresponding experimental observations both in the SC-state^{24–29} and the pseudogap-state^{30–36}, and therefore further confirm that the QSI octet phenomenology both in the pseudogap phase and SC-state and the checkerboard charge ordering in the pseudogap phase are the intrinsic phenomena in cuprate superconductors free from any set-point-related issues.

In cuprate superconductors, the impurity distribution accompanied with different types of the doping processes are quite different^{16–18}. In particular, the atomic dislocation in the charge-carrier doping process gives rise to impurities in the insulating layers, which often act as smooth scatterers because of the poor screening effects along the direction normal to the CuO_2 planes. For instance, for the cuprate superconductors $(\text{Bi,Pb})_2(\text{Sr,L a})_2\text{CuO}_{6+\delta}$ and $\text{Bi}_2\text{Sr}_{1.6}\text{L}_{0.4}\text{CuO}_{6+\delta}$ ($\text{L}=\text{La,Nd,Gd}$), the mismatch in the ionic radius between Bi and Pb or Sr and L leads to that the effective impurities reside in the insulating layers^{89–92} with distances away from the conducting CuO_2 planes, where the concentration of the out-of-plane impurities is controlled by varying the radius of the Pb or L ions. As in the case of the SC-state⁶³, the intrinsic phenomena of the QSI octet phenomenology and the checkerboard charge ordering in the pseudogap phase should be manifested regardless of the impurity distribution. To confirm this point more clearly, we now discuss the modulation of the ratio of LDOS at opposite energy (then the LDOS modulation) in the presence of an out-of-plane impurity.

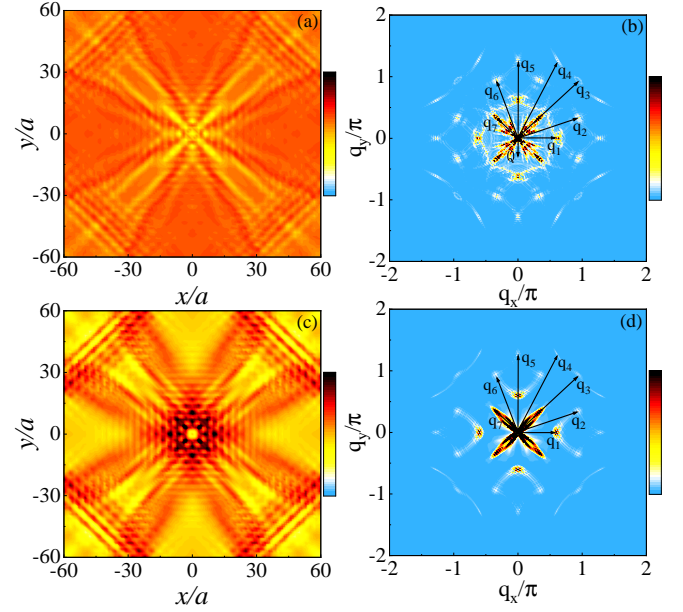


FIG. 7. (Color online) Upper panel: the intensity maps of the ratio of the local density of states at opposite energy in the pseudogap phase for an out-of-plane single impurity in (a) real-space and (b) momentum-space at doping $\delta = 0.09$ with temperature $T = 0.07J$ in the binding-energy $\omega = 0.06J$ for the impurity-scattering strength $V_s = 1.0J$ and screening length $L = 1.0a$. Lower panel: the corresponding intensity maps of the ratio of the local density of states at opposite energy in the superconducting-state for an out-of-plane single impurity in (c) real-space and (d) momentum-space with temperature $T = 0.002J$.

For an out-of-plane single impurity located at the lattice site $\mathbf{r} = 0$, the smooth impurity-scattering potential in real-space can be modeled as⁹³,

$$V(\mathbf{r}) = V_s e^{-\mathbf{r}/L}, \quad (38)$$

with the out-of-plane impurity-scattering strength V_s and screening length L , respectively, and then this impurity-scattering potential in momentum-space can be derived straightforwardly by using the Fourier transformation as,

$$V_{\mathbf{k}\mathbf{k}'} = \frac{2\pi V_s/L}{[(\mathbf{k} - \mathbf{k}')^2 + 1/L^2]^{3/2}}. \quad (39)$$

In the following discussions, these out-of-plane impurity-scattering strength V_s and screening length L in Eqs. (38) and (39) are set as $V_s = 1.0J$ and $L = 1.0a$, respectively.

In the upper panel of Fig. 7, we plot the intensity maps of the ratio of the LDOS at opposite energy in the pseudogap phase in (a) real-space and (b) momentum-space at doping $\delta = 0.09$ with temperature $T = 0.07J$ in the binding-energy $\omega = 0.06J$ for the impurity-scattering strength $V_s = 1.0J$ and screening length $L = 1.0a$. For a direct comparison, the corresponding intensity maps of the ratio of LDOS at opposite energy in the SC-state in (c) real-space and (d) momentum-space with

temperature $T = 0.002J$ are plotted in the lower panel of Fig. 7. In comparison with the corresponding results obtained for an in-plane single impurity shown in Fig. 6, it thus shows that the main features of the δZ modulations both in the pseudogap phase and SC-state for an out-of-plane single impurity are essentially the same as the corresponding ones for an in-plane single impurity. In particular, as a natural consequence of the quasiparticle scattering geometry that is directly governed by the shape of the constant energy contour and the related octet scattering model shown in Fig. 2, (i) the scattering wave vectors \mathbf{q}_i obey the octet scattering model, in spite of various forms of the impurity scattering potentials; (ii) the main feature of QSI is similar to that for an in-plane single impurity as shown in Fig. 6; (iii) the essential behaviours of QSI peak dispersions for an out-of-plane single impurity are almost the same as those for an in-plane single impurity as shown in Fig. 4, and also coincide with the evolution of the constant energy contour and the related octet scattering model in Fig. 2 with energy; (iv) the non-dispersive nature of the checkerboard charge ordering in the pseudogap phase and the related magnitude of the checkerboard charge-order wave vector $|\mathbf{Q}|$ are the same as those for an in-plane single impurity regardless of various forms of the impurity scattering potentials. However, there are some subtle differences between the δZ modulations for an out-of-plane single impurity and an in-plane single impurity: (i) the real-space $\delta Z(\mathbf{r}, \omega)$ modulations in both the pseudogap phase and SC-state for an out-of-plane single impurity are more pronounced than the corresponding ones for an in-plane single impurity, and this difference is also reflected in the momentum-space $\delta Z(\mathbf{q}, \omega)$ modulations, where the weights of the QSI peaks both in the pseudogap phase and SC-state for an out-of-plane single impurity are larger than these for an in-plane single impurity, indicating that QSI in the underdoped cuprate superconductors may be generated mainly by both the strong electron correlation and out-of-plane single impurity scattering. On the other hand, the weight of the checkerboard peaks in the pseudogap phase for an out-of-plane single impurity is smaller than that for an in-plane single impurity, which shows that the effects both from the strong electron correlation and the in-plane single impurity scattering play the crucial role for the checkerboard ordering in the pseudogap phase; (ii) the shape of the $\delta Z(\mathbf{q}, \omega)$ modulation pattern in the pseudogap phase for an out-of-plane single impurity deviates modestly from the rotundity-like shape of the $\delta Z(\mathbf{q}, \omega)$ modulation pattern for an in-plane single impurity. These results therefore confirm that the essential features of the QSI octet phenomenology both in the pseudogap phase and SC-state as well as the checkerboard charge ordering in the pseudogap phase are the intrinsic phenomena regardless of the impurity distribution.

In the recent discussion of the nature of QSI in the SC-state⁶³, we have shown that the overall

feature of the LDOS modulation in the SC-state can be depicted qualitatively by taking into account the quasiparticle scattering from a single impurity on the kinetic-energy-driven homogeneous SC-state, however, the pronounced QSI peaks in the momentum-space LDOS modulation for a single impurity are smeared heavily for multiple impurities, and then the momentum-space LDOS modulation for multiple impurities exhibits a speckle pattern. In this case, we have also discussed the LDOS modulation in the pseudogap phase for multiple impurities, and the obtained results show that as in the case of the SC-state, although the pronounced QSI peaks and the checkerboard peaks in the momentum-space LDOS modulation for a single impurity are also smeared heavily for multiple impurities, the characteristic structure of the LDOS modulation spectrum are essentially the same both for multiple impurities and a single impurity.

Now we try to give an explanation to show (i) why the characteristic of QSI observed in the SC-state remains unchanged upon passing above T_c in the pseudogap phase? and (ii) why the non-dispersive checkerboard charge ordering emerges in the pseudogap phase only? The nature of the LDOS modulation is mainly governed by the momentum-space profiles of the joint density of states. Although the SC-state of the underdoped cuprate superconductors coexists and competes with the pseudogap-state, the SC-state quasiparticle still exhibits the particle-hole mixing^{94,95} similar to that in the conventional superconductors^{96,97}. In particular, in the low-energy limit, the quasiparticle energy dispersion $\varpi_{\mathbf{k}}(\omega)$ in Eq. (11a) in the SC-state can be reduced as⁷³, $\varpi_{\mathbf{k}} = E_{\mathbf{k}}$, where $E_{\mathbf{k}} = \sqrt{\bar{\varepsilon}_{\mathbf{k}}^2 + |\bar{\Delta}_{\mathbf{z}\mathbf{k}}|^2}$, with $\bar{\varepsilon}_{\mathbf{k}} = Z_F \varepsilon_{\mathbf{k}}$, and $\bar{\Delta}_{\mathbf{z}\mathbf{k}} = Z_F \bar{\Delta}_{\mathbf{k}}$, while the single-particle coherent weight Z_F that is directly associated with the normal-state pseudogap has been given explicitly in Ref. 73. In this case, the scattering wave vector \mathbf{q}_i obeying the octet scattering model dominates the LDOS modulation at energy ω , since these \mathbf{k} -pairs on the constant energy contour shown in Fig. 2b connected by the scattering wave vector \mathbf{q}_i have a high joint density of states. This also follows from a basic fact that the magnitude of the SC gap $|\bar{\Delta}_{\mathbf{k}}|$ is momentum-dependent, and then some different minima ω_i , at which the quasiparticles emerge, occur at the tips of the Fermi arcs²⁴⁻²⁹. However, the square-lattice CuO_2 plane has a four-fold rotation symmetry, which implies that at any non-zero energy ω_i , there are only eight possible \mathbf{k}_F values at which $|\bar{\Delta}_{\mathbf{z}\mathbf{k}}| = \omega_i$ in the first Brillouin zone²⁴⁻²⁹. The highest joint density of states for the quasiparticle scattering at this energy ω_i occur at \mathbf{q}_i -vectors connecting the eight tips of the Fermi arcs. This is why the SC-state QSI peaks in the momentum-space LDOS modulation occur at these \mathbf{q}_i -vectors. However, the existence of the QSI octet phenomenology in the pseudogap phase is not very surprised, since all the behaviours of the QSI octet phenomenology observed in the STM/S experiments are

closely related to the momentum-space profiles of the joint density of states^{37–42}, while the main feature of the momentum-space profiles of the joint density of states in the pseudogap phase^{30–36} characterized by the octet scattering model shown in Fig. 2a is almost the same as that in the SC-state^{24–29} shown in Fig. 2b. In other words, the main feature of the joint density of states occurred in the SC-state survive virtually unchanged into the pseudogap phase, which leads to that the SC-state QSI octet phenomenology exists in the pseudogap phase. However, the spectral weight at around the antinodal region in the SC-state is gapped out by both the normal-state pseudogap and the d-wave SC gap, while the spectral weight at around the antinodal region in the pseudogap phase is suppressed partially by the normal-state pseudogap only, resulting in the existence of small residual weight at around the antinodal region in the pseudogap phase. In this case, the checkerboard charge ordering in the SC-state is suppressed strongly by both the normal-state pseudogap and SC gap, leading to that the checkerboard charge ordering in the SC-state becomes unobservable in experiments, while this checkerboard charge ordering in the pseudogap phase is suppressed partially by the normal-state pseudogap, leading to that the checkerboard charge ordering in the pseudogap phase becomes observable in experiments. This is why the checkerboard peaks in the momentum-space LDOS modulation occur in the pseudogap phase only.

V. SUMMARY

Within the framework of the kinetic-energy-driven superconductivity, we have rederived the homogeneous electron propagator, where the strong coupling between electrons directly from the kinetic energy by the exchange of the spin excitation induces the pseudogap-state in the particle-hole channel and the SC-state in the particle-particle channel. The pseudogap and the SC gap respectively originate from the electron normal self-energy in the particle-hole channel and the electron anomalous self-energy in the particle-particle channel, and are obtained explicitly by taking into account the vertex correction. This pseudogap-state coexists and competes with the SC-state below T_c , leading to a dome-like shape of the doping dependence of T_c , and the exotic pseudogap phase with the normal-state pseudogap persisting up to T^* that is substantially higher than T_c in the underdoped regime. Moreover, the structure of the constant energy contour intensity maps

in the pseudogap phase essentially coincides with the corresponding one in the SC-state, where the pseudogap suppresses strongly the spectral weight on the constant energy contour at around the antinodal region, while it suppresses modestly the spectral weight at around the nodal region, leading to the formation of the Fermi arcs centered around the nodal region. These tips of the Fermi arcs connected by the quasiparticle scattering wave vectors \mathbf{q}_i naturally construct an octet scattering model. Starting from the microscopic homogeneous electron propagator and the related octet scattering model, we have studied the nature of the LDOS modulation in the pseudogap phase of cuprate superconductors within the T -matrix approach, where the T -matrix generated by the quasiparticle scattering from various kinds of a single impurity is derived accurately, and is employed to derive LDOS by the involvement of all the quasiparticle excitations and scattering processes. Our results show a number of anomalous electronic-state properties in the pseudogap phase of cuprate superconductors is directly correlated to the opening of the normal-state pseudogap: (i) as a natural consequence of the same characteristic of the octet scattering model both in the SC-state and pseudogap phase, the QSI octet phenomenology in the SC-state survive virtually unchanged into the pseudogap phase; (ii) however, the electronic density of states on the constant energy contour at around the antinodal region in the SC-state is gapped out completely by both the d-wave SC gap and normal-state pseudogap, while it in the pseudogap phase is depressed partially by the normal-state pseudogap, which directly leads to that the non-dispersive checkerboard charge ordering with a finite wave vector \mathbf{Q} emerges in the pseudogap phase only. Our results in this paper together with the previous work for QSI in the SC-state⁶³ therefore show that the electronic-state affected by the normal-state pseudogap exhibit the LDOS modulation spectrum organization.

ACKNOWLEDGEMENTS

X.L. and S.P. are supported by the National Key Research and Development Program of China under Grant Nos. 2023YFA1406500 and 2021YFA1401803, and the National Natural Science Foundation of China (NSFC) under Grant No. 12274036. M.Z. is supported by NSFC under Grant No. 12504172 and the Special Funding for Postdoctoral Research Projects in Chongqing under Grant No. 2024CQBSHTB3156. H.G. acknowledge support from NSFC under grant No. 12574249.

Appendix A: Derivation of T -matrix in the pseudogap phase

In this Appendix, we follow the previous derivation of the T -matrix in the SC-state⁶³ to evaluate accurately the T -matrix in the pseudogap phase. The T -matrix in Eq. (23b) of the main text can be expressed explicitly in terms of the equation of iteration method as,

$$T_{\mathbf{k}\mathbf{k}'}(\omega) = \frac{1}{N}V_{\mathbf{k}\mathbf{k}'} + \frac{1}{N}\sum_{\mathbf{k}_1}V_{\mathbf{k}\mathbf{k}_1}G(\mathbf{k}_1,\omega)\frac{1}{N}V_{\mathbf{k}_1\mathbf{k}'} + \frac{1}{N}\sum_{\mathbf{k}_1}V_{\mathbf{k}\mathbf{k}_1}G(\mathbf{k}_1,\omega)\frac{1}{N}\sum_{\mathbf{k}_2}V_{\mathbf{k}_1\mathbf{k}_2}G(\mathbf{k}_2,\omega)\frac{1}{N}V_{\mathbf{k}_2\mathbf{k}'} + \cdots, \quad (\text{A1})$$

which can be derived straightforwardly as⁶³,

$$T_{\mathbf{k}\mathbf{k}'}(\omega) = \left(\bar{V} \frac{1}{1 - \bar{M}} \right)_{\mathbf{k}\mathbf{k}'}, \quad (\text{A2})$$

where $\bar{V} = V/N$ is a matrix, N is the number of lattice sites, while the matrix \bar{M} can be obtained explicitly as,

$$\bar{M} = \begin{pmatrix} G(\mathbf{k}_1, \omega)\bar{V}_{\mathbf{k}_1\mathbf{k}_1} & G(\mathbf{k}_1, \omega)\bar{V}_{\mathbf{k}_1\mathbf{k}_2} & G(\mathbf{k}_1, \omega)\bar{V}_{\mathbf{k}_1\mathbf{k}_3} & \cdots & G(\mathbf{k}_1, \omega)\bar{V}_{\mathbf{k}_1\mathbf{k}_N} \\ G(\mathbf{k}_2, \omega)\bar{V}_{\mathbf{k}_2\mathbf{k}_1} & G(\mathbf{k}_2, \omega)\bar{V}_{\mathbf{k}_2\mathbf{k}_2} & G(\mathbf{k}_2, \omega)\bar{V}_{\mathbf{k}_2\mathbf{k}_3} & \cdots & G(\mathbf{k}_2, \omega)\bar{V}_{\mathbf{k}_2\mathbf{k}_N} \\ \vdots & \vdots & \vdots & \vdots & \vdots \\ G(\mathbf{k}_N, \omega)\bar{V}_{\mathbf{k}_N\mathbf{k}_1} & G(\mathbf{k}_N, \omega)\bar{V}_{\mathbf{k}_N\mathbf{k}_2} & G(\mathbf{k}_N, \omega)\bar{V}_{\mathbf{k}_N\mathbf{k}_3} & \cdots & G(\mathbf{k}_N, \omega)\bar{V}_{\mathbf{k}_N\mathbf{k}_N} \end{pmatrix}. \quad (\text{A3})$$

However, the T -matrix in Eq. (23b) of the main text can be also derived directly as,

$$T(\omega) = \bar{V} + \bar{M}(\omega)T(\omega) = \frac{1}{1 - \bar{M}(\omega)}\bar{V}, \quad (\text{A4})$$

with the matrix,

$$\bar{M} = \begin{pmatrix} \bar{V}_{\mathbf{k}_1\mathbf{k}_1}G(\mathbf{k}_1, \omega) & \bar{V}_{\mathbf{k}_1\mathbf{k}_2}G(\mathbf{k}_2, \omega) & \bar{V}_{\mathbf{k}_1\mathbf{k}_3}G(\mathbf{k}_3, \omega) & \cdots & \bar{V}_{\mathbf{k}_1\mathbf{k}_N}G(\mathbf{k}_N, \omega) \\ \bar{V}_{\mathbf{k}_2\mathbf{k}_1}G(\mathbf{k}_1, \omega) & \bar{V}_{\mathbf{k}_2\mathbf{k}_2}G(\mathbf{k}_2, \omega) & \bar{V}_{\mathbf{k}_2\mathbf{k}_3}G(\mathbf{k}_3, \omega) & \cdots & \bar{V}_{\mathbf{k}_2\mathbf{k}_N}G(\mathbf{k}_N, \omega) \\ \vdots & \vdots & \vdots & \vdots & \vdots \\ \bar{V}_{\mathbf{k}_N\mathbf{k}_1}G(\mathbf{k}_1, \omega) & \bar{V}_{\mathbf{k}_N\mathbf{k}_2}G(\mathbf{k}_2, \omega) & \bar{V}_{\mathbf{k}_N\mathbf{k}_3}G(\mathbf{k}_3, \omega) & \cdots & \bar{V}_{\mathbf{k}_N\mathbf{k}_N}G(\mathbf{k}_N, \omega) \end{pmatrix}. \quad (\text{A5})$$

* E-mail: mhzeng@cqu.edu.cn

† E-mail: spfeng@bnu.edu.cn

¹ See, e.g., the review, B. Keimer, S. A. Kivelson, M. R. Norman, S. Uchida, and J. Zaanen, From quantum matter to high-temperature superconductivity in copper oxides, *Nature* **518**, 179 (2015).

² See, e.g., the review, C. M. Varma, Colloquium: Linear in temperature resistivity and associated mysteries including high temperature superconductivity, *Rev. Mod. Phys.* **92**, 031001 (2020).

³ See, e.g., the review, N. E. Hussey, High-temperature superconductivity and strange metallicity: Simple observations with (possibly) profound implications, *Physica C* **614**, 1354362 (2023).

⁴ See, e.g., the review, T. Timusk and B. Statt, The pseudogap in high-temperature superconductors: an experimental survey, *Rep. Prog. Phys.* **62**, 61 (1999).

⁵ See, e.g., the review, S. Hüfner, M. A. Hossain, A. Damascelli, and G. A. Sawatzky, Two gaps make a high-temperature superconductor? *Rep. Prog. Phys.* **71**, 062501 (2008).

⁶ See, e.g., the review, A. Damascelli, Z. Hussain, and Z.-X.

Shen, Angle-resolved photoemission studies of the cuprate superconductors, *Rev. Mod. Phys.* **75**, 473 (2003).

⁷ See, e.g., the review, J. C. Campuzano, M. R. Norman, M. Randeria, Photoemission in the high- T_c superconductors, in *Physics of Superconductors*, vol. II, edited by K. H. Bennemann and J. B. Ketterson (Springer, Berlin Heidelberg New York, 2004), p. 167.

⁸ See, e.g., the review, J. Fink, S. Borisenko, A. Kordyuk, A. Koitzsch, J. Geck, V. Zabolotnyy, M. Knupfer, B. Büchner, and H. Berger, Dressing of the charge carriers in high- T_c superconductors, in *Lecture Notes in Physics*, vol. 715, edited by S. Hüfner (Springer-Verlag Berlin Heidelberg, 2007), p. 295.

⁹ N. E. Hussey, What drives pseudogap physics in high- T_c cuprates? A view from the (resistance) bridge, *J. Phys. Chem. Solids* **72**, 529 (2011).

¹⁰ See, e.g., the review, I. M. Vishik, Photoemission perspective on pseudogap, superconducting fluctuations, and charge order in cuprates: a review of recent progress, *Rep. Prog. Phys.* **81**, 062501 (2018).

¹¹ I. K. Drozdov, I. Pletikosić, C. -K. Kim, K. Fujita, G. D. Gu, J. C. S. Davis, P. D. Johnson, I. Božović, and T.

- Valla, Phase diagram of $\text{Bi}_2\text{Sr}_2\text{CaCu}_2\text{O}_{8+\delta}$ revisited, *Nat. Commun.* **9**, 5210 (2018).
- ¹² See, e.g., the review, M. Fujita, H. Hiraka, M. Matsuda, M. Matsuura, J. M. Tranquada, S. Wakimoto, G. Xu, and K. Yamada, Progress in neutron scattering studies of spin excitations in high- T_c cuprates, *J. Phys. Soc. Jpn.* **81**, 011007 (2012).
 - ¹³ P. W. Anderson, The resonating valence bond state in La_2CuO_4 and superconductivity, *Science* **235**, 1196 (1987).
 - ¹⁴ J. G. Bednorz and K. A. Müller, Possible high T_c superconductivity in the Ba-La-Cu-O system, *Z. Phys. B* **64**, 189 (1986).
 - ¹⁵ M. K. Wu, J. R. Ashburn, C. J. Torng, P. H. Hor, R. L. Meng, L. Gao, Z. J. Huang, Y. Q. Wang, and C. W. Chu, Superconductivity at 93 K in a new mixed-phase Y-Ba-Cu-O compound system at ambient pressure, *Phys. Rev. Lett.* **58**, 908 (1987).
 - ¹⁶ See, e.g., the review, N. E. Hussey, Low-energy quasiparticles in high- T_c cuprates, *Adv. Phys.* **51**, 1685 (2002).
 - ¹⁷ See, e.g., the review, A. V. Balatsky, I. Vekhter, and J.-X. Zhu, Impurity-induced states in conventional and unconventional superconductors, *Rev. Mod. Phys.* **78**, 373 (2006).
 - ¹⁸ See, e.g., the review, H. Alloul, J. Bobroff, M. Gabay, and P. J. Hirschfeld, Defects in correlated metals and superconductors, *Rev. Mod. Phys.* **81**, 45 (2009).
 - ¹⁹ S. H. Pan, J. P. ÓNeal, R. L. Badzey, C. Chamon, H. Ding, J. R. Engelbrecht, Z. Wang, H. Eisaki, S. Uchida, A. K. Gupta, K.-W. Ng, E. W. Hudson, K. M. Lang, and J. C. Davis, Microscopic electronic inhomogeneity in the high- T_c superconductor $\text{Bi}_2\text{Sr}_2\text{CaCu}_2\text{O}_{8+x}$, *Nature* **413**, 282 (2001).
 - ²⁰ See, e.g., the review, Ø. Fischer, M. Kugler, I. Maggio-Aprile, C. Berthod, and C. Renner, Scanning tunneling spectroscopy of high-temperature superconductors, *Rev. Mod. Phys.* **79**, 353 (2007).
 - ²¹ See, e.g., the review, J.-X. Yin, S. H. Pan, and M. Z. Hasan, Probing topological quantum matter with scanning tunnelling microscopy, *Nat. Rev. Phys.* **3**, 249 (2021).
 - ²² M. Zeng, X. Li, Y. Wang, and S. Feng, Influence of impurities on electronic structure in cuprate superconductors, *Phys. Rev. B* **106**, 054512 (2022).
 - ²³ M. Zeng, X. Li, Y. Wang, and S. Feng, Microwave conductivity due to impurity scattering in cuprate superconductors, *Phys. Rev. B* **108**, 094505 (2023).
 - ²⁴ S. H. Pan, E. W. Hudson, K. M. Lang, H. Eisaki, S. Uchida, and J. C. Davis, Imaging the effects of individual zinc impurity atoms on superconductivity in $\text{Bi}_2\text{Sr}_2\text{CaCu}_2\text{O}_{8+\delta}$, *Nature* **403**, 746 (2000).
 - ²⁵ J. E. Hoffman, E. W. Hudson, K. M. Lang, V. Madhavan, H. Eisaki, S. Uchida, and J. C. Davis, Imaging quasiparticle interference in $\text{Bi}_2\text{Sr}_2\text{CaCu}_2\text{O}_{8+\delta}$, *Science* **297**, 1148 (2002).
 - ²⁶ K. McElroy, R. W. Simmonds, J. E. Hoffman, D.-H. Lee, J. Orenstein, H. Eisaki, S. Uchida, and J. C. Davis, Relating atomic-scale electronic phenomena to wave-like quasiparticle states in superconducting $\text{Bi}_2\text{Sr}_2\text{CaCu}_2\text{O}_{8+\delta}$, *Nature* **422**, 592 (2003).
 - ²⁷ Y. Kohsaka, C. Taylor, P. Wahl, A. Schmidt, J. Lee, K. Fujita, J. W. Alldredge, K. McElroy, J. Lee, H. Eisaki, S. Uchida, D.-H. Lee, and J. C. Davis, How Cooper pairs vanish approaching the Mott insulator in $\text{Bi}_2\text{Sr}_2\text{CaCu}_2\text{O}_{8+\delta}$, *Nature* **454**, 1072 (2008).
 - ²⁸ T. Hanaguri, Y. Kohsaka, M. Ono, M. Maltseva, P. Coleman, I. Yamada, M. Azuma, M. Takano, K. Ohishi, and H. Takagi, Coherence factors in a high- T_c cuprate probed by quasi-particle scattering off vortices, *Science* **323**, 923 (2009).
 - ²⁹ I. M. Vishik, E. A. Nowadnick, W. S. Lee, Z. X. Shen, B. Moritz, T. P. Devereaux, K. Tanaka, T. Sasagawa, and T. Fujii, A momentum-dependent perspective on quasiparticle interference in $\text{Bi}_2\text{Sr}_2\text{CaCu}_2\text{O}_{8+\delta}$, *Nat. Phys.* **5**, 718 (2009).
 - ³⁰ M. Vershinin, S. Misra, S. Ono, Y. Abe, Y. Ando, A. Yazdani, Local ordering in the pseudogap state of the high- T_c superconductor $\text{Bi}_2\text{Sr}_2\text{CaCu}_2\text{O}_{8+\delta}$, *Science* **303**, 1995 (2004).
 - ³¹ T. Hanaguri, C. Lupien, Y. Kohsaka, D.-H. Lee, M. Azuma, M. Takano, H. Takagi, and J. C. Davis, A 'checkerboard' electronic crystal state in lightly hole-doped $\text{Ca}_{2-x}\text{Na}_x\text{CuO}_2\text{Cl}_2$, *Nature* **430**, 1001 (2004).
 - ³² K. McElroy, D.-H. Lee, J. E. Hoffman, K. M. Lang, J. Lee, E. W. Hudson, H. Eisaki, S. Uchida, and J. C. Davis, Coincidence of checkerboard charge order and antinodal state decoherence in strongly underdoped superconducting $\text{Bi}_2\text{Sr}_2\text{CaCu}_2\text{O}_{8+\delta}$, *Phys. Rev. Lett.* **94**, 197005 (2005).
 - ³³ W. D. Wise, M. C. Boyer, K. Chatterjee, T. Kondo, T. Takeuchi, H. Ikuta, Y. Wang, E. W. Hudson, Charge density wave origin of cuprate checkerboard visualized by scanning tunneling microscopy, *Nat. Phys.* **4**, 696 (2008).
 - ³⁴ J. Lee, K. Fujita, A. R. Schmidt, C. K. Kim, H. Eisaki, S. Uchida, and J. C. Davis, Spectroscopic fingerprint of phase-incoherent superconductivity in the underdoped $\text{Bi}_2\text{Sr}_2\text{CaCu}_2\text{O}_{8+\delta}$, *Science* **325**, 1099 (2009).
 - ³⁵ A. R. Schmidt, K. Fujita, E.-A. Kim, M. J. Lawler, H. Eisaki, S. Uchida, D.-H. Lee, and J. C. Davis, Electronic structure of the cuprate superconducting and pseudogap phases from spectroscopic imaging STM, *New J. Phys.* **13**, 065014 (2011).
 - ³⁶ K. Fujita, M. H. Hamidian, S.D. Edkins, Chung Koo Kim, Y. Kohsaka, M. Azuma, M. Takano, H. Takagi, H. Eisaki, S. Uchida, A. Allais, M. J. Lawler, E.-A. Kim, S. Sachdev, and J. C. S. Davis, Direct phase-sensitive identification of a d -form factor density wave in underdoped cuprates, *Proc. Natl. Acad. Sci. USA* **111**, E3026-E3032 (2014).
 - ³⁷ U. Chatterjee, M. Shi, A. Kaminski, A. Kanigel, H. M. Fretwell, K. Terashima, T. Takahashi, S. Rosenkranz, Z. Z. Li, H. Raffy, A. Santander-Syro, K. Kadowaki, M. R. Norman, M. Randeria, and J. C. Campuzano, Nondispersive Fermi arcs and the absence of charge ordering in the pseudogap phase of $\text{Bi}_2\text{Sr}_2\text{CaCu}_2\text{O}_{8+\delta}$, *Phys. Rev. Lett.* **96**, 107006 (2006).
 - ³⁸ K. McElroy, G.-H. Gweon, S. Y. Zhou, J. Graf, S. Uchida, H. Eisaki, H. Takagi, T. Sasagawa, D.-H. Lee, and A. Lanzara, Elastic scattering susceptibility of the high temperature superconductor $\text{Bi}_2\text{Sr}_2\text{CaCu}_2\text{O}_{8+\delta}$: a comparison between real and momentum space photoemission spectroscopies, *Phys. Rev. Lett.* **96**, 067005 (2006).
 - ³⁹ U. Chatterjee, M. Shi, A. Kaminski, A. Kanigel, H. M. Fretwell, K. Terashima, T. Takahashi, S. Rosenkranz, Z. Z. Li, H. Raffy, A. Santander-Syro, K. Kadowaki, M. Randeria, M. R. Norman, and J. C. Campuzano, Anomalous dispersion in the autocorrelation of angle-resolved photoemission spectra of high-temperature $\text{Bi}_2\text{Sr}_2\text{CaCu}_2\text{O}_{8+\delta}$ superconductors, *Phys. Rev. B* **76**,

- 012504 (2007).
- ⁴⁰ Y. He, Y. Yin, M. Zech, A. Soumyanarayanan, M. M. Yee, T. Williams, M. C. Boyer, K. Chatterjee, W. D. Wise, I. Zeljkovic, T. Kondo, T. Takeuchi, H. Ikuta, P. Mistark, R. S. Markiewicz, A. Bansil, S. Sachdev, E. W. Hudson, and J. E. Hoffman, Fermi surface and pseudogap evolution in a cuprate superconductor, *Science* **344**, 608 (2014).
 - ⁴¹ F. Restrepo, J. Zhao, J. C. Campuzano, and U. Chatterjee, Temperature and carrier concentration dependence of Fermi arcs in moderately underdoped $\text{Bi}_2\text{Sr}_2\text{CaCu}_2\text{O}_{8+\delta}$ cuprate high-temperature superconductors: A joint density of states perspective, *Phys. Rev. B* **107**, 174519 (2023).
 - ⁴² N. K. Shah, J. Zhao, and U. Chatterjee, Particle-hole symmetry in the pseudogap phase of moderately underdoped cuprate high temperature superconductors evidenced from joint density of states analysis, arXiv:2509.12568.
 - ⁴³ See, e.g., the review, R. Comin and A. Damascelli, Resonant x-ray scattering studies of charge order in cuprates, *Annu. Rev. Condens. Matter Phys.* **7**, 369 (2016).
 - ⁴⁴ R. Comin, A. Frano, M. M. Yee, Y. Yoshida, H. Eisaki, E. Schierle, E. Weschke, R. Sutarto, F. He, A. Soumyanarayanan, Yang He, M. L. Tacon, I. S. Elfimov, Jennifer E. Hoffman, G. A. Sawatzky, B. Keimer, and A. Damascelli, Charge order driven by Fermi-arc instability in $\text{Bi}_2\text{Sr}_{2-x}\text{La}_x\text{CuO}_{6+\delta}$, *Science* **343**, 390 (2014).
 - ⁴⁵ G. Ghiringhelli, M. Le Tacon, M. Minola, S. Blanco-Canosa, C. Mazzoli, N. B. Brookes, G. M. De Luca, A. Frano, D. G. Hawthorn, F. He, T. Loew, M. M. Sala, D. C. Peets, M. Salluzzo, E. Schierle, R. Sutarto, G. A. Sawatzky, E. Weschke, B. Keimer, and L. Braicovich, Long-range incommensurate charge fluctuations in $(\text{Y,Nd})\text{Ba}_2\text{Cu}_3\text{O}_{6+x}$, *Science* **337**, 821 (2012).
 - ⁴⁶ E. H. da Silva Neto, P. Aynajian, A. Frano, R. Comin, E. Schierle, E. Weschke, A. Gyenis, J. Wen, J. Schneeloch, Z. Xu, S. Ono, G. Gu, M. Le Tacon, and A. Yazdani, Ubiquitous interplay between charge ordering and high-temperature superconductivity in cuprates, *Science* **343**, 393 (2014).
 - ⁴⁷ G. Campi, A. Bianconi, N. Poccia, G. Bianconi, L. Barba, G. Arrighetti, D. Innocenti, J. Karpinski, N. D. Zhigadlo, S. M. Kazakov, M. Burghammer, M. v. Zimmermann, M. Sprung and A. Ricci, Inhomogeneity of charge-density-wave order and quenched disorder in a high- T_c superconductor, *Nature* **525**, 359 (2015).
 - ⁴⁸ M. Hashimoto, E. A. Nowadnick, R.-H. He, I. M. Vishik, B. Moritz, Y. He, K. Tanaka, R. G. Moore, D. Lu, Y. Yoshida, M. Ishikado, T. Sasagawa, K. Fujita, S. Ishida, S. Uchida, H. Eisaki, Z. Hussain, T. P. Devereaux, and Z.-X. Shen, Direct spectroscopic evidence for phase competition between the pseudogap and superconductivity in $\text{Bi}_2\text{Sr}_2\text{CaCu}_2\text{O}_{8+\delta}$, *Nat. Mater.* **14**, 37 (2015).
 - ⁴⁹ D. S. Dessau, B. O. Wells, Z.-X. Shen, W. E. Spicer, A. J. Arko, R. S. List, D. B. Mitzi, and A. Kapitulnik, Anomalous spectral weight transfer at the superconducting transition of $\text{Bi}_2\text{Sr}_2\text{CaCu}_2\text{O}_{8+\delta}$, *Phys. Rev. Lett.* **66**, 2160 (1991).
 - ⁵⁰ J. C. Campuzano, H. Ding, M. R. Norman, H. M. Fretwell, M. Randeria, A. Kaminski, J. Mesot, T. Takeuchi, T. Sato, T. Yokoya, T. Takahashi, T. Mochiku, K. Kadowaki, P. Guptasarma, D. G. Hinks, Z. Konstantinovic, Z. Z. Li, and H. Raffy, Electronic spectra and their relation to the (π, π) collective mode in high- T_c superconductors, *Phys. Rev. Lett.* **83**, 3709 (1999).
 - ⁵¹ D. H. Lu, D. L. Feng, N. P. Armitage, K. M. Shen, A. Damascelli, C. Kim, F. Ronning, Z.-X. Shen, D. A. Bonn, R. Liang, W. N. Hardy, A. I. Rykov, and S. Tajima, Superconducting gap and strong in-plane anisotropy in untwinned $\text{YBa}_2\text{Cu}_3\text{O}_{7\delta}$, *Phys. Rev. Lett.* **86**, 4370 (2001).
 - ⁵² T. Sato, H. Matsui, S. Nishina, T. Takahashi, T. Fujii, T. Watanabe, and A. Matsuda, Low energy excitation and scaling in $\text{Bi}_2\text{Sr}_2\text{Ca}_{n-1}\text{Cu}_n\text{O}_{2n+4}$ ($n = 1 - 3$): Angle-resolved photoemission spectroscopy, *Phys. Rev. Lett.* **89**, 067005 (2002).
 - ⁵³ S. V. Borisenko, A. A. Kordyuk, T. K. Kim, A. Koitzsch, M. Knupfer, M. S. Golden, J. Fink, M. Eschrig, H. Berger, and R. Follath, Anomalous enhancement of the coupling to the magnetic resonance mode in underdoped Pb-Bi2212 , *Phys. Rev. Lett.* **90**, 207001 (2003).
 - ⁵⁴ J. Wei, Y. Zhang, H. W. Ou, B. P. Xie, D. W. Shen, J. F. Zhao, L. X. Yang, M. Arita, K. Shimada, H. Namatame, M. Taniguchi, Y. Yoshida, H. Eisaki, and D. L. Feng, Superconducting coherence peak in the electronic excitations of a single-layer $\text{Bi}_2\text{Sr}_{1.6}\text{La}_{0.4}\text{CuO}_{6+\delta}$ cuprate superconductor, *Phys. Rev. Lett.* **101**, 097005 (2008).
 - ⁵⁵ B. Loret, S. Sakai, S. Benhabib, Y. Gallais, M. Cazayous, M. A. Méasson, R. D. Zhong, J. Schneeloch, G. D. Gu, A. Forget, D. Colson, I. Paul, M. Civelli, and A. Sacuto, Vertical temperature boundary of the pseudogap under the superconducting dome in the phase diagram of $\text{Bi}_2\text{Sr}_2\text{CaCu}_2\text{O}_{8+\delta}$, *Phys. Rev. B* **96**, 094525 (2017).
 - ⁵⁶ D. Mou, A. Kaminski, and G. Gu, Direct observation of self-energy signatures of the resonant collective mode in $\text{Bi}_2\text{Sr}_2\text{CaCu}_2\text{O}_{8+\delta}$, *Phys. Rev. B* **95**, 174501 (2017).
 - ⁵⁷ P. V. Bogdanov, A. Lanzara, S. A. Kellar, X. J. Zhou, E. D. Lu, W. J. Zheng, G. Gu, J.-I. Shimoyama, K. Kishio, H. Ikeda, R. Yoshizaki, Z. Hussain, and Z. X. Shen, Evidence for an energy scale for quasiparticle dispersion in $\text{Bi}_2\text{Sr}_2\text{CaCu}_2\text{O}_8$, *Phys. Rev. Lett.* **85**, 2581 (2000).
 - ⁵⁸ A. Kaminski, M. Randeria, J. C. Campuzano, M. R. Norman, H. Fretwell, J. Mesot, T. Sato, T. Takahashi, and K. Kadowaki, Renormalization of spectral line shape and dispersion below T_c in $\text{Bi}_2\text{Sr}_2\text{CaCu}_2\text{O}_{8+\delta}$, *Phys. Rev. Lett.* **86**, 1070 (2001).
 - ⁵⁹ P. D. Johnson, T. Valla, A. V. Fedorov, Z. Yusof, B. O. Wells, Q. Li, A. R. Moodenbaugh, G. D. Gu, N. Koshizuka, C. Kendziora, S. Jian, and D. G. Hinks, Doping and temperature dependence of the mass enhancement observed in the cuprate $\text{Bi}_2\text{Sr}_2\text{CaCu}_2\text{O}_{8+\delta}$, *Phys. Rev. Lett.* **87**, 177007 (2001).
 - ⁶⁰ T. Sato, H. Matsui, T. Takahashi, H. Ding, H.-B. Yang, S.-C. Wang, T. Fujii, T. Watanabe, A. Matsuda, T. Terashima, and K. Kadowaki, Observation of band renormalization effects in hole-doped high- T_c superconductors, *Phys. Rev. Lett.* **91**, 157003 (2003).
 - ⁶¹ W. S. Lee, K. Tanaka, I. M. Vishik, D. H. Lu, R. G. Moore, H. Eisaki, A. Iyo, T. P. Devereaux, and Z. X. Shen, Dependence of band-renormalization effects on the number of copper oxide layers in Tl-based copper oxide superconductors revealed by angle-resolved photoemission spectroscopy, *Phys. Rev. Lett.* **103**, 067003 (2009).
 - ⁶² J. He, W. Zhang, J. M. Bok, D. Mou, L. Zhao, Y. Peng, S. He, G. Liu, X. Dong, J. Zhang, J. S. Wen, Z. J. Xu, G. D. Gu, X. Wang, Q. Peng, Z. Wang, S. Zhang, F. Yang, C. Chen, Z. Xu, H.-Y. Choi, C. M. Varma, and X. J. Zhou,

- Coexistence of two sharp-mode couplings and their unusual momentum dependence in the superconducting state of $\text{Bi}_2\text{Sr}_2\text{CaCu}_2\text{O}_{8+\delta}$ revealed by laser-based angle-resolved photoemission, *Phys. Rev. Lett.* **111**, 107005 (2013).
- ⁶³ M. Zeng, X. Li, Y. Wang, and S. Feng, Quasiparticle scattering interference in cuprate superconductors, *Phys. Rev. B* **110**, 134523 (2024).
- ⁶⁴ See, e.g., the review, L. Yu, Many-body problems in high temperature superconductivity, in *Recent Progress in Many-Body Theories*, edited by T. L. Ainsworth, C. E. Campbell, B. E. Clements, and E. Krotscheck (Plenum, New York, 1992), Vol. **3**, p. 157.
- ⁶⁵ S. Feng, J. B. Wu, Z. B. Su, and L. Yu, Slave-particle studies of the electron-momentum distribution in the low-dimensional t - J model, *Phys. Rev. B* **47**, 15192 (1993).
- ⁶⁶ L. Zhang, J. K. Jain, and V. J. Emery, Importance of the local constraint in slave-boson theories, *Phys. Rev. B* **47**, 3368 (1993).
- ⁶⁷ See, e.g., the review, P. A. Lee, N. Nagaosa, and X.-G. Wen, Doping a Mott insulator: Physics of high-temperature superconductivity, *Rev. Mod. Phys.* **78**, 17 (2006).
- ⁶⁸ S. Feng, J. Qin, and T. Ma, A gauge invariant dressed holon and spinon description of the normal state of underdoped cuprates, *J. Phys.: Condens. Matter* **16**, 343 (2004); S. Feng, Z. B. Su, and L. Yu, Fermion-spin transformation to implement the charge-spin separation, *Phys. Rev. B* **49**, 2368 (1994).
- ⁶⁹ See, e.g., the review, S. Feng, Y. Lan, H. Zhao, L. Kuang, L. Qin, and X. Ma, Kinetic-energy-driven superconductivity in cuprate superconductors, *Int. J. Mod. Phys. B* **29**, 1530009 (2015).
- ⁷⁰ S. Feng, Kinetic energy driven superconductivity in doped cuprates, *Phys. Rev. B* **68**, 184501 (2003); S. Feng, T. Ma, and H. Guo, Magnetic nature of superconductivity in doped cuprates, *Physica C* **436**, 14 (2006).
- ⁷¹ S. Feng, H. Zhao, and Z. Huang, Two gaps with one energy scale in cuprate superconductors, *Phys. Rev. B* **85**, 054509 (2012); *Phys. Rev. B* **85**, 099902(E) (2012).
- ⁷² S. Feng, L. Kuang, and H. Zhao, Electronic structure of cuprate superconductors in a full charge-spin recombination scheme, *Physica C* **517**, 5 (2015).
- ⁷³ X. Li, M. Zeng, H. Guo, and S. Feng, Unusual electronic structure in underdoped cuprate superconductors, *Physica C* **636**, 1354767 (2025).
- ⁷⁴ J. R. Schrieffer, Ward's identity and the suppression of spin fluctuation superconductivity, *J. Low Temp. Phys.* **99**, 397 (1995).
- ⁷⁵ K.-J. Xu, Q. Guo, M. Hashimoto, Z.-X. Li, S.-D. Chen, J. He, Y. He, C. Li, M. H. Berntsen, C. R. Rotundu, Y. S. Lee, T. P. Devereaux, A. Rydh, D.-H. Lu, D.-H. Lee, O. Tjernberg, Z.-X. Shen, Bogoliubov quasiparticle on the gossamer Fermi surface in electron-doped cuprates, *Nat. Phys.* **19**, 1834 (2023).
- ⁷⁶ L. N. Cooper, Bound electron pairs in a degenerate Fermi gas, *Phys. Rev.* **104**, 1189 (1956).
- ⁷⁷ M. R. Norman, H. Ding, M. Randeria, J. C. Campuzano, T. Yokoya, T. Takeuchi, T. Takahashi, T. Mochiku, K. Kadowaki, P. Guptasarma, and D. G. Hinks, Destruction of the Fermi surface in underdoped high- T_c superconductors, *Nature* **392**, 157 (1998).
- ⁷⁸ M. Shi, J. Chang, S. Pailh  s, M. R. Norman, J. C. Campuzano, M. M  nsson, T. Claesson, O. Tjernberg, A. Bendounan, L. Patthey, N. Momono, M. Oda, M. Ido, C. Mudry, and J. Mesot, Coherent d -wave superconducting gap in underdoped $\text{La}_{2-x}\text{Sr}_x\text{CuO}_4$ by angle-resolved photoemission spectroscopy, *Phys. Rev. Lett.* **101**, 047002 (2008).
- ⁷⁹ Y. Sassa, M. Radovi  , M. M  nsson, E. Razzoli, X. Y. Cui, S. Pailh  s, S. Guerrero, M. Shi, P. R. Willmott, F. Miletto Granozio, J. Mesot, M. R. Norman, and L. Patthey, Ortho-II band folding in $\text{YBa}_2\text{Cu}_3\text{O}_{7-\delta}$ films revealed by angle-resolved photoemission, *Phys. Rev. B* **83**, 140511(R) (2011).
- ⁸⁰ M. Horio, T. Adachi, Y. Mori, A. Takahashi, T. Yoshida, H. Suzuki, L. C. C. Ambolode II, K. Okazaki, K. Ono, H. Kumigashira, H. Anzai, M. Arita, H. Namatame, M. Taniguchi, D. Ootsuki, K. Sawada, M. Takahashi, T. Mizokawa, Y. Koike, and A. Fujimori, Suppression of the antiferromagnetic pseudogap in the electron-doped high-temperature superconductor by protect annealing, *Nat. Commun.* **7**, 10567 (2016).
- ⁸¹ B. Loret, Y. Gallais, M. Cazayous, R. D. Zhong, J. Schneeloch, G. D. Gu, A. Fedorov, T. K. Kim, S. V. Borisenko, and A. Sacuto, Raman and ARPES combined study on the connection between the existence of the pseudogap and the topology of the Fermi surface in $\text{Bi}_2\text{Sr}_2\text{CaCu}_2\text{O}_{8+\delta}$, *Phys. Rev. B* **97**, 174521 (2018).
- ⁸² C. E. Matt, C. G. Fatuzzo, Y. Sassa, M. M  nsson, S. Fatale, V. Bitetta, X. Shi, S. Pailh  s, M. H. Berntsen, T. Kurosawa, M. Oda, N. Momono, O. J. Lipscombe, S. M. Hayden, J.-Q. Yan, J.-S. Zhou, J. B. Goodenough, S. Pyon, T. Takayama, H. Takagi, L. Patthey, A. Bendounan, E. Razzoli, M. Shi, N. C. Plumb, M. Radovic, M. Grioni, J. Mesot, O. Tjernberg, and J. Chang, Electron scattering, charge order, and pseudogap physics in $\text{La}_{1.6-x}\text{Nd}_{0.4}\text{Sr}_x\text{CuO}_4$: An angle-resolved photoemission spectroscopy study, *Phys. Rev. B* **92**, 134524 (2015).
- ⁸³ D. Gao, Y. Mou, Y. Liu, S. Tan, and S. Feng, Autocorrelation of quasiparticle spectral intensities and its connection with quasiparticle scattering interference in cuprate superconductors, *Phil. Mag.* **99**, 752 (2019).
- ⁸⁴ Y. Liu, Y. Lan, and S. Feng, Peak structure in the self-energy of cuprate superconductors, *Phys. Rev. B* **103**, 024525 (2021); S. Tan, Y. Liu, Y. Mou, and S. Feng, Anisotropic dressing of electrons in electron-doped cuprate superconductors, *Phys. Rev. B* **103**, 014503 (2021).
- ⁸⁵ K. M. Shen, F. Ronning, D. H. Lu, F. Baumberger, N. J. C. Ingle, W. S. Lee, W. Meevasana, Y. Kohsaka, M. Azuma, M. Takano, H. Takagi, and Z.-X. Shen, Nodal quasiparticles and antinodal charge ordering in $\text{Ca}_{2-x}\text{Na}_x\text{CuO}_2\text{Cl}_2$, *Science* **307**, 901 (2005).
- ⁸⁶ Y. Kohsaka, C. Taylor, K. Fujita, A. Schmidt, C. Lupien, T. Hanaguri, M. Azuma, M. Takano, H. Eisaki, H. Takagi, S. Uchida, and J. C. Davis, An intrinsic bond-centered electronic glass with unidirectional domains in underdoped cuprates, *Science* **315**, 1380 (2007).
- ⁸⁷ T. Hanaguri, Y. Kohsaka, J. C. Davis, C. Lupien, I. Yamada, M. Azuma, M. Takano, K. Ohishi, M. Ono, H. Takagi, Quasi-particle interference and superconducting gap in a high-temperature superconductor $\text{Ca}_{2-x}\text{Na}_x\text{CuO}_2\text{Cl}_2$, *Nature Phys.* **3**, 865 (2007).
- ⁸⁸ Z. Wang, B. Liu, and S. Feng, Extinction of quasiparticle scattering interference in cuprate superconductors, *Phys. Lett. A* **374**, 3084 (2010).
- ⁸⁹ H. Eisaki, N. Kaneko, D. L. Feng, A. Damascelli, P. K. Mang, K. M. Shen, Z.-X. Shen, and M. Greven, Effect

- of chemical inhomogeneity in bismuth-based copper oxide superconductors, *Phys. Rev. B* **69**, 064512 (2004).
- ⁹⁰ K. Fujita, T. Noda, K. M. Kojima, H. Eisaki, and S. Uchida, Effect of disorder outside the CuO_2 planes on T_c of copper oxide superconductors, *Phys. Rev. Lett.* **95**, 097006 (2005).
- ⁹¹ T. Kondo, T. Takeuchi, A. Kaminski, S. Tsuda, and S. Shin, Evidence for two energy scales in the superconducting state of optimally doped $(\text{Bi,Pb})_2(\text{Sr,Lu})_2\text{CuO}_{6+\delta}$, *Phys. Rev. Lett.* **98**, 267004 (2007).
- ⁹² M. Hashimoto, T. Yoshida, A. Fujimori, D. H. Lu, Z.-X. Shen, M. Kubota, K. Ono, M. Ishikado, K. Fujita, and S. Uchida, Effects of out-of-plane disorder on the nodal quasiparticle and superconducting gap in single-layer $\text{Bi}_2\text{Sr}_{1.6}\text{Lu}_{0.4}\text{CuO}_{6+\delta}$ ($\text{L}=\text{La,Nd,Gd}$), *Phys. Rev. B* **79**, 144517 (2009).
- ⁹³ T. S. Nunner, W. Chen, B. M. Andersen, A. Melikyan, and P. J. Hirschfeld, Fourier transform spectroscopy of d -wave quasiparticles in the presence of atomic scale pairing disorder, *Phys. Rev. B* **73**, 104511 (2006).
- ⁹⁴ J. C. Campuzano, H. Ding, M. R. Norman, M. Randeria, A. F. Bellman, T. Yokoya, T. Takahashi, H. Katayama-Yoshida, T. Mochiku, and K. Kadowaki, Direct observation of particle-hole mixing in the superconducting state by angle-resolved photoemission, *Phys. Rev. B* **53**, R14737 (1996).
- ⁹⁵ H. Matsui, T. Sato, T. Takahashi, S.-C. Wang, H.-B. Yang, H. Ding, T. Fujii, T. Watanabe, and A. Matsuda, BCS-like Bogoliubov quasiparticles in high- T_c superconductors observed by angle-resolved photoemission spectroscopy, *Phys. Rev. Lett.* **90**, 217002 (2003).
- ⁹⁶ J. Bardeen, L. N. Cooper, and J. R. Schrieffer, Theory of superconductivity, *Phys. Rev.* **108**, 1175 (1957).
- ⁹⁷ See, e.g., J. R. Schrieffer, *Theory of Superconductivity*, Benjamin, New York, 1964.